

Structural evolution of the reactivated Møre–Trøndelag Fault Complex, Fosen Peninsula, Norway



Lee M. Watts^{1,2}, Robert E. Holdsworth^{1,3*}, David Roberts⁴, Janine M. Sleight^{1,2} and Richard J. Walker⁵




¹ Department of Earth Sciences, Durham University, Science Labs, Durham DH1 3LE, UK

² Shell UK Ltd, 1 Altens Farm Road, Nigg, Aberdeen AB12 3FY, UK

³ Geospatial Research Limited, Office Suite 7, Harrison House, 1 Hawthorn Terrace, Durham DH1 4EL, UK

⁴ Geological Survey of Norway, Leiv Eirikssons vei 39, 7040 Trondheim, Norway

⁵ Department of Earth & Planetary Sciences, University of California Davis, Davis, CA 95616, USA

 REH, 0000-0002-3467-835X

* Correspondence: r.e.holdsworth@durham.ac.uk

Abstract: The ENE–WSW-trending Møre–Trøndelag Fault Complex (MTFC) in Central Norway is a 10–50 km-wide, steeply dipping reactivated fault zone. Onshore, it transects Devonian sedimentary rocks and a series of east to SE transported metamorphic nappes, which were emplaced during the Scandian (Silurian–Devonian) Orogeny. Offshore, the MTFC defines the southern margin of the Møre Basin and the northern margin of the Viking Graben, meaning that the fault complex played a major role in controlling the architecture of these Mesozoic basins. Onshore, the MTFC has had a prolonged and heterogeneous kinematic history. The complex comprises two major fault strands: the Hitra–Snåsa Fault (HSF) and the Verran Fault (VF). These two faults seem to have broadly initiated as part of a single system of sinistral ductile shear zones during the early Devonian (c. 410 Ma). Sinistral transtensional reactivation (Permo–Carboniferous; 290 Ma) of the ENE–WSW-trending HSF and VF led to the development of cataclasites and pseudotachylites together with the formation of north–south-trending faults establishing the present-day brittle fault geometry of the MTFC. Later phases of Mesozoic reactivation focused along the Verran Fault Zone (VFZ) and north–south-linking structures were probably related to mid- to late Jurassic to early Cretaceous rifting and late Cretaceous to early Cenozoic opening of the North Atlantic.

Supplementary material: Supplementary datasets are available at <https://doi.org/10.6084/m9.figshare.c.6390518>

Thematic collection: This article is part of the Caledonian Wilson cycle collection available at: <https://www.lyellcollection.org/topic/collections/the-caledonian-wilson-cycle>

Received 5 October 2022; revised 9 January 2023; accepted 16 January 2023

The important role played by multiply reactivated, deep-seated faults in controlling basin development in rifted margins has been widely discussed (e.g. Doré *et al.* 1997; Holdsworth *et al.* 1997; Manatschal *et al.* 2014; Phillips *et al.* 2016). In many cases, these structures extend from offshore areas into onshore regions where direct field- and laboratory-based observations of fault geometry, kinematic history, fault rock character, microstructure, evolution and potential weakening mechanisms are possible (e.g. Imber *et al.* 2001; Wilson *et al.* 2006, 2010). The Møre–Trøndelag Fault Complex (MTFC; Fig. 1a–c; Gabrielsen and Ramberg 1979; Roberts 1983; Grønlie and Roberts 1989; Grønlie *et al.* 1991; Séranne 1992; Watts 2001; Braathen *et al.* 2002; Redfield *et al.* 2005a, b; Osmundsen *et al.* 2006; Olsen *et al.* 2007; Peron-Pinvidic and Osmundsen 2020) in the Norwegian Caledonides is an outstanding example of such a fault zone. This 10–50 km-wide, ENE–WSW-trending, steeply dipping to subvertical composite structure has a strike length of >300 km in Central Norway, extending offshore and southwestwards into the northern limits of the Viking Graben where it has been suggested to link with the fault systems of Shetland and the Scottish mainland (Fig. 1a; Norton *et al.* 1987; Grønlie and Roberts 1989; Doré *et al.* 1997; Watts *et al.* 2007). The MTFC forms a key structure related to both orogen-parallel displacements and top-to-the-west Devonian extension in the Norwegian Caledonides (e.g. Braathen *et al.* 2000, 2002; Nordgulen *et al.* 2002; Osmundsen *et al.* 2003; Steltenpohl *et al.* 2011; Ksienzyk *et al.* 2014; Peron-Pinvidic and Osmundsen 2020).

In this contribution, we detail the kinematic, textural and microstructural history and evolution of the MTFC in the well-exposed Fosen Peninsula just NW of Trondheimsfjord (Fig. 1b and c). We discuss the regional implications for the tectonic evolution of the Norwegian continental margin and our understanding of reactivated continental fault zones.

Regional setting

The Fosen Peninsula (Fig. 1b) forms part of the Western Gneiss Region, where some of the deepest crustal levels of the Caledonide orogen are exposed. In terms of Scandinavian Caledonian tectonostratigraphy (Roberts and Gee 1985), the geology is dominated by Paleoproterozoic, migmatized, granitic and granodioritic complexes of the Lower Allochthon, which were intensely reworked into foliated, banded gneisses and locally re-migmatized during the main Caledonian, Scandian orogenesis in Late Silurian to Early Devonian time (Johansson 1986; Roberts 1986). The informal term ‘Banded Gneiss Complex’ has been applied to the rocks of this terrane (Möller 1988). Also present in some areas are Neoproterozoic to Ordovician supracrustal rocks of far-travelled thrust sheets of the Middle and Upper allochthons (Fig. 1b; Solli *et al.* 1997; Roberts and Stephens 2000; Tucker *et al.* 2004; Hollocher *et al.* 2012). Devonian conglomerates and sandstones occur locally (e.g. Siedlecka 1975; Steel *et al.* 1985; Bøe and Sturt 1991; Haabesland 2002), and the youngest exposed formation is

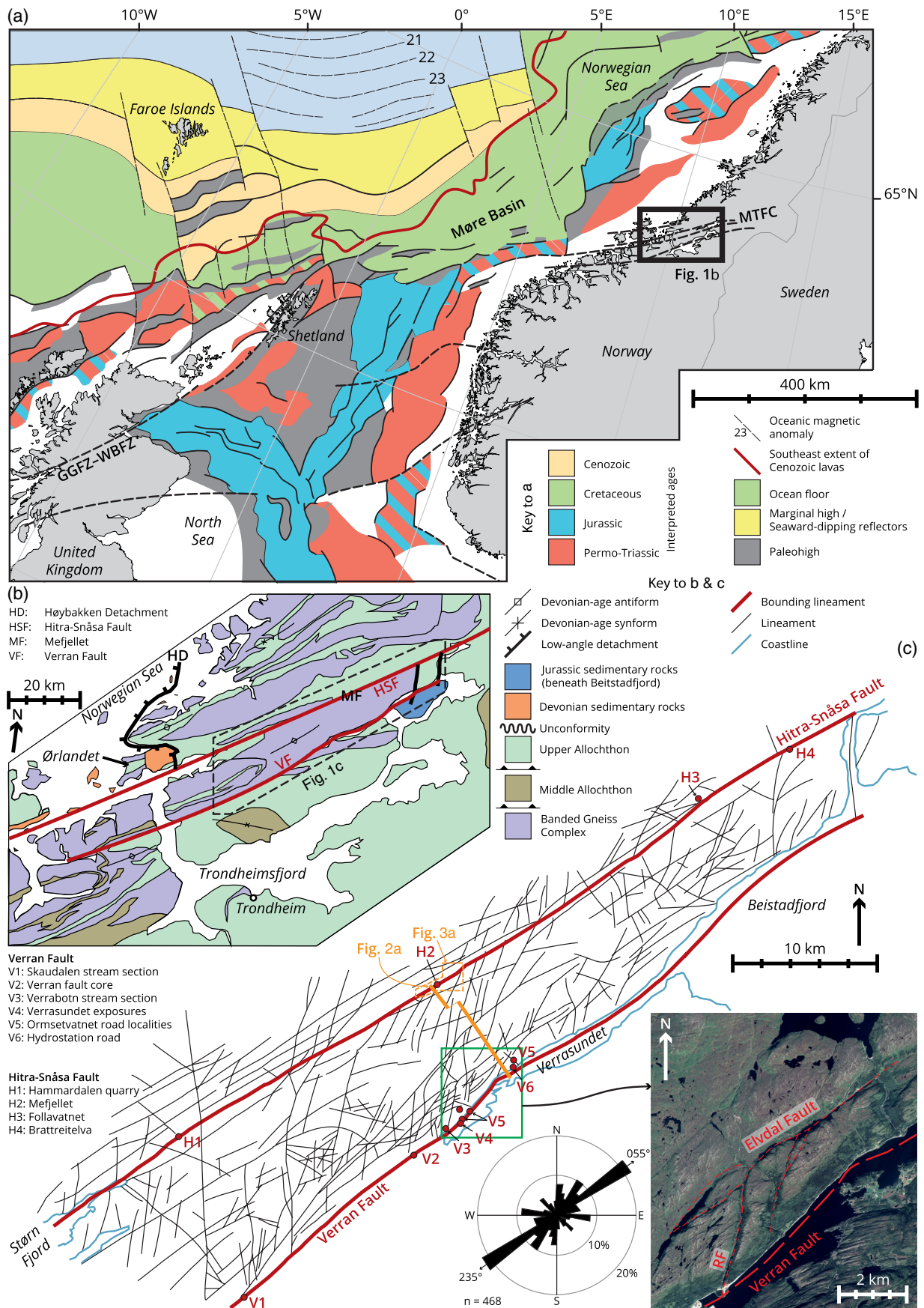


Fig. 1. (a) Map showing location and regional context of the Fosen Peninsula (outlined by box, **(b)**) and the major offshore basins of the NE Atlantic rifted margin (after Doré *et al.* 1997). WBFZ, Walls Boundary Fault Zone; GGFZ, Great Glen Fault Zone; MTFC, More-Trondelag Fault Complex. (b) Simplified geological map of the Fosen area, Central Norway. Map area shown in **(c)** is outlined by dashed box. (c) Lineament map from interpretation of Landsat image of the Fosen Peninsula NW of Trondheimsfjord, with specific locations named in the main text indicated and location of cross-section in Figure 2a. Green box shows location of aerial image shown in bottom right, with main faults highlighted. Rose diagram shows fault lineament trends. Dashed orange box outlines mapped area shown in Figure 3a.

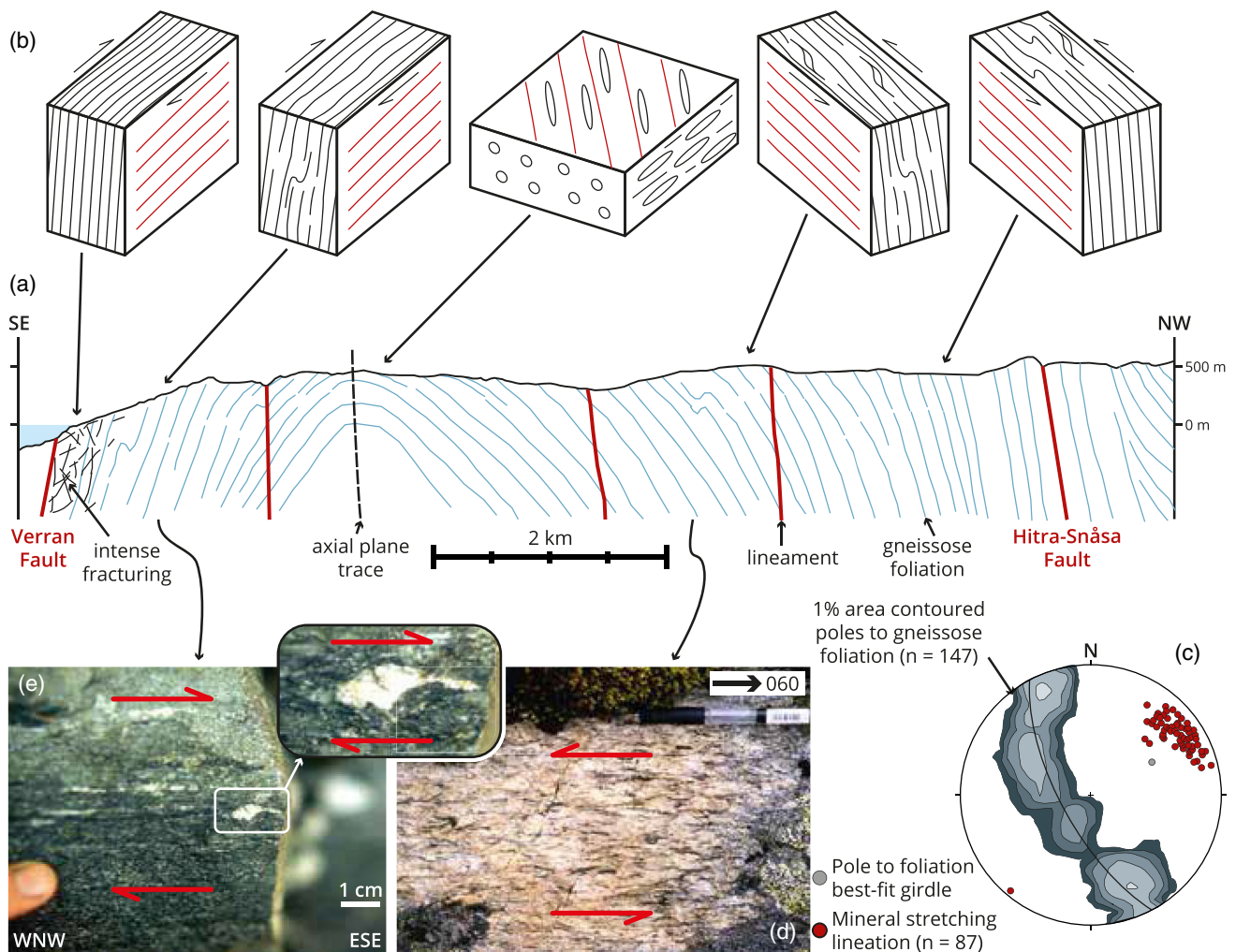


Fig. 2. (a) Simplified SE–NW cross-section across the MTFC (location shown in Fig. 1c) showing regional antiform that predates faulting. (b) Schematic summary of tectonic fabrics and associated shear senses found in different domains across the fold; L-tectonites in the hinge should be noted. (c) Equal area lower hemisphere stereonet showing contours of poles to gneissose foliation and mineral stretching lineations. (d) and (e) show plan views of gneissose fabrics with sinistral and dextral shear criteria, from the NW and SE fold limbs, respectively.

now considered to be of Early Carboniferous age (Eide *et al.* 2005). Although not exposed onshore, seismic-reflection profiling has shown that Jurassic sedimentary rocks are present in a half-graben in Beitstadfjorden (Fig. 1b), juxtaposed against one of the main faults of the MTFC (Bøe and Bjerkli 1989; Sommaruga and Bøe 2002). Other small, shallow, Jurassic basins have been reported from nearshore areas along the fault complex to the SW of Fosen Peninsula (e.g. Sommaruga and Bøe 2002; Bøe *et al.* 2010).

On Fosen, the MTFC postdates the stacking of the Caledonian nappes and thrust sheets and comprises two main steeply dipping structures 10–20 km apart, the Hitra–Snåsa Fault (HSF) and Verran Fault (VF), and a third oblique structure, the Mosvik Fault (Grønlie and Roberts 1989; Grønlie *et al.* 1991, 1994). To the NE, the two principal faults merge into a single structure that transects the antiformal Grong–Olden Culmination with diminishing offset and eventually appears to die out in a horsetail splay with an array of east–west-trending faults (Roberts 1998). The low-angle Høybakkken detachment (Fig. 1b) lies to the NW of the HSF and developed synchronously with the deposition of lower to middle Devonian sedimentary rocks (Séranne 1992; Robinson *et al.* 2004; Osmundsen *et al.* 2006). Directly SE of Fosen Peninsula, an inferred fault along a near-vertical, submerged escarpment in Trondheimsfjord has also been considered to be a part of the fault complex, and this idea has received support from identification of the Bæverdalen lineament or fault, SW of Trondheim, and other faults inland from Kristiansund (Redfield *et al.* 2005a; Nasuti *et al.* 2011).

The long-lived, reactivated character of the MTFC has been confirmed by a wealth of isotopic and fission-track data (e.g. Piasecki and Cliff 1988; Grønlie *et al.* 1990, 1991, 1994; 2005a, b; Kendrick *et al.* 2004; Redfield *et al.* 2004; Sherlock *et al.* 2004; Tucker *et al.* 2004; Eide *et al.* 2005; Hestnes *et al.* 2022; Tartaglia *et al.* 2022). Although there is a possibility that precursor faults may have existed in the Paleoproterozoic basement prior to the collision between Baltica and Laurentia that produced the Scandian Orogeny (Grønlie and Roberts 1989; Séranne 1992), the earliest isotopically dated movement along the faults is that of ductile sinistral strike-slip in Early Devonian time (Kendrick *et al.* 2004). Subsequently, there were further phases of strike-slip, oblique-slip and dip-slip of varying magnitude in the latest Devonian, early Permian to Triassic, late Jurassic and late Cretaceous or early Cenozoic (e.g. Grønlie *et al.* 1990, 1994; Redfield *et al.* 2004, 2005a; Sherlock *et al.* 2004; Hestnes *et al.* 2022; Tartaglia *et al.* 2022). There is widespread evidence for hydrothermal and metasomatic alteration associated with the MTFC represented mostly by multi-stage mineral veining, thorium-enriched breccias and cataclasites. The main mineralizing events are thought to be of Permian, late Jurassic and late Cretaceous to early Cenozoic age (Grønlie and Torsvik 1989; Grønlie *et al.* 1990, 1994). The hydrothermal fluids vary in chemistry through time, resulting in striking geochemical anomalies and the precipitation of complex and locally dense mineral vein networks both along the faults and in the adjacent

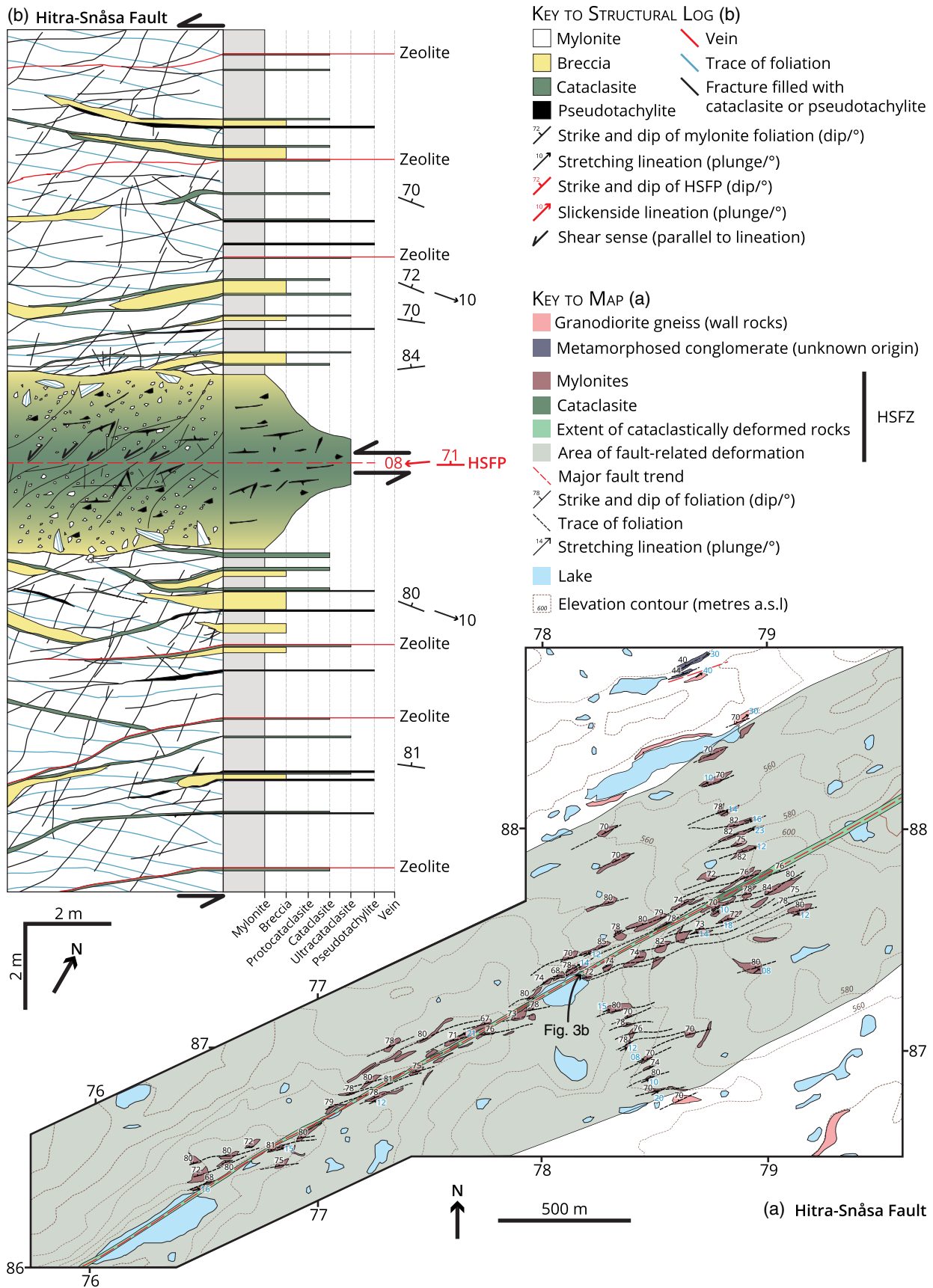


Fig. 3. (a) Detailed geological map of the HSFZ in the Mefjellet area (location shown in Fig. 1c), also showing location of (b). (b) Structural log from the core of the HSFZ at map reference 32V NR 7796 8719 to illustrate overprinting relationships, fault rock distributions and structure. HSFP, Hitra-Snåsa Fault Plane.

country rocks (Grønlie *et al.* 1991; Watts 2001; Sæther *et al.* 2005). The principal mineral phases are calcite, zeolite (stilbite and laumontite), epidote, prehnite, quartz and fluorite.

Recent attention has focused on the latest Cretaceous to Cenozoic uplift of the southern Scandes Mountains and the likely role played by the MTFC in controlling the development of the so-called ‘Great

Escarpment' between Kristiansund and Ålesund (Lidmar-Bergström *et al.* 2000; Redfield *et al.* 2004, 2005a, b; Redfield and Osmundsen 2009, 2013; Ksienzyk *et al.* 2014; Fossen *et al.* 2017). Fission-track dating in transects across the escarpment has revealed evidence for a latest Cretaceous to Cenozoic, NW-side down, cumulative normal reactivation of up to 2–3 km with displacements decreasing markedly towards Trondheimsfjord and the Fosen Peninsula in the NE (Redfield *et al.* 2005a). Moreover, the blocks between the different faults each appear to record disparate exhumation histories (Redfield *et al.* 2004). The MTFC also marks a boundary between crustal blocks with differing present-day stress fields (Roberts and Myrvang 2004; Pascal *et al.* 2010). Seismically, the Fosen Peninsula district is relatively quiescent, but the 'Great Escarpment' along-strike to the SW is one of the most seismically active regions of mainland Norway (Hicks *et al.* 2000).

Field and laboratory methods

Fieldwork studied deformation structures related to the MTFC affecting the Banded Gneiss Complex and associated early Paleozoic intrusions of Fosen in a series of key localities where exposure is good (Fig. 1b and c). The relative ages of country rock fabrics, igneous intrusions, mineral veins and fault rocks were ascertained from observed cross-cutting relationships. Structural geometries and kinematic relationships were recorded through collection of orientation and displacement vector data. Structural data were collected using compass–clinometers supplemented with orientation data derived from interpreted aerial and satellite imagery (e.g. Fig. 1c). Shear zone and later faulting kinematics were determined using ductile (asymmetric shear zone fabrics, porphyroclasts and S–C fabrics; e.g. Passchier and Trouw 2005) and brittle (offsets of identified piercing points, en echelon veins and slickenline steps; e.g. Petit 1987) shear sense criteria. A representative sample set of oriented hand specimens were collected for thin sectioning. Transmitted light microscopy and backscattered electron microscopy were used to study petrography, microstructures and overprinting relationships.

In the regional synthesis, we have calculated moment tensor (P – T) strain axes from compiled fault slickenline data for two of the main events documented using Faultkin 8 (see Marrett and Allmendinger 1990; Allmendinger *et al.* 2012). The structural datasets used are given in the Supplementary material. Previous studies have used fault slickenline data for palaeostress inversion (e.g. Tartaglia *et al.* 2022), in which it is assumed that the principal stress and strain axes are parallel. This assumption strictly applies to isotropic media rather than for foliated rocks and fault reactivation, and this is an important limitation in the use of such approaches. To compare our calculated strains with palaeostress inversion analyses using this assumption, the maximum elongation axis ϵ_1 would represent the minimum compressive stress σ_3 , and the maximum shortening axis ϵ_3 would represent the maximum compressive stress σ_1 .

The MTFC on the Fosen Peninsula

Protolith lithologies and structures

The gneissose rocks forming the Banded Gneiss Complex of Fosen are well exposed in the region separating the HSF and VF (Fig. 1c). They are derived from Late Paleoproterozoic, granitic–tonalitic orthogneisses and are cross-cut by a number of Ordovician to Early Silurian diorite and granite bodies (Tucker *et al.* 2004). Both the gneisses and the intrusions were intensely reworked into L–S tectonites during Scandian deformation and metamorphism (Roberts 1998). The pink–grey, fine- to coarse-grained gneisses are typically equigranular, with grain sizes ranging from 0.5 to 1 cm. They comprise perthitic microcline, plagioclase (An_{55-5}) and quartz

(70–80% of the rock), secondary epidote (after calcic plagioclase), chlorite, biotite, muscovite, hornblende, garnet, kyanite and titanite, together with accessory magnetite and pyrite. Compositional banding, mainly on millimetre scales, is defined by variations in the relative abundances of the main minerals, particularly quartz and feldspar. An ENE–WSW-trending subvertical fabric and subhorizontal lineation are defined mainly by flattened and elongated aggregates of quartz and feldspar. Centimetre- to metre-thick amphibolite sheets occur locally, and generally lie parallel to the gneissose foliation.

Ordovician–Early Silurian granites are exposed south of Verrasundet and in a stream section at Skaudalen (Fig. 1c). They are grey in colour and medium to coarse grained with phenocrysts of plagioclase and orthoclase up to 3 cm in length. Typically, they are composed of c. 40% orthoclase, 30% plagioclase, 20% quartz and 10% biotite together with minor amounts of disseminated oxides and epidote grains. Feldspars are replaced by aggregates of sericite, giving rise to a speckled appearance. The granites contain an ENE–WSW-trending foliation defined by flattened and stretched aggregates of quartz and feldspar. Lineations defined by elongate feldspar and quartz plunge shallowly to the SW.

A well-exposed section between Mefjellet and Trongundet in the region separating the HSF and VF illustrates the regional structure of the gneisses (Fig. 2a and b). The foliation here is folded into a kilometre-scale, ENE-plunging antiform, the hinge of which lies parallel to the ubiquitous mineral stretching lineation (Fig. 2c), although minor fold hinges in the antiform core are locally observed to lie up to 20° clockwise of the linear fabric. According to the regional transtensional deformation model of Krabbendam and Dewey (1998), these upright folds were generated during low-angle, top-to-the-WSW shear accompanied by constrictional strain, leading to differential exhumation of the gneisses within the fold core, with sinistral shear on the NW fold limb and dextral shear on the SE fold limb (Fig. 2b, d and e), as indicated by asymmetrically wrapped feldspar porphyroblasts (σ -type) and centimetre-scale shear-band fabrics.

MTFC structures and associated fault-rock assemblages

The Hitra–Snåsa Fault Zone

The Hitra–Snåsa Fault Zone (HSFZ) is a zone of intense brittle–ductile deformation best exposed in a narrow ENE–WSW-oriented linear valley cutting the Mefjellet area, a hilly region located north of the Ormsetvatnet reservoir (Figs 1c and 3a). Here, the HSFZ is a 1.4 km-wide ductile shear zone containing mylonites with a narrow 20 m-thick central fault core containing widespread cataclasis and pseudotachylite (Fig. 3b). In places, millimetre-thick calcite and zeolite veins transect the cataclases, and are almost entirely localized along pre-existing fractures. Other less well-exposed sections through the HSFZ have been described in detail by Watts (2001).

Shear-zone mylonites. At distances of up to 750 m either side of the central fault core a protomylonitic fabric overprints granitic or granodiorite gneiss. Increasingly fine-grained platy mylonites (Fig. 4a) become dominant over protomylonitic fabrics towards the core, with anastomosing high-strain zones, 2–50 m thick, surrounding low-strain zones. Foliation-parallel quartz veins (Fig. 4b; 2–50 cm thick) are common and most abundant in the 100 m closest to the central fault core. Foliation-parallel, variably mylonitized pegmatites, 5 cm to 1 m thick, occur up to 450 m from the core and increase in frequency towards it. At distances of less than 150 m from the core, ENE–WSW-oriented, 20 cm- to 1 m-thick dykes of mylonitized microdiorite are preserved and increase in frequency towards the fault core. Some are deformed by metre-scale isoclinal folds with subhorizontal hinges.

Mylonites derived from other protoliths are also locally present. For example, 400 m NW of the central fault core, grey–green mylonites derived from polymict conglomerates are preserved, and very similar grey–green mylonites derived from interleaved slivers of psammites (Fig. 4c), marbles and schists lie to the SE of the central fault trace in Brattreitelva. Along-strike and to the NE, a series of spectacular marble mylonites are interlayered with phyllonites derived from schists (Watts 2001).

Foliations in the HSFZ of the Mefjellet area follow a general ENE–WSW trend with steep NW dips (Fig. 5, top row). Lineations defined by elongate quartz, feldspar and aligned micas plunge shallowly to the ENE. Feldspar porphyroclasts 1 mm to 1 cm across typically display σ - and δ -type geometries consistent with sinistral shear when viewed on horizontal outcrop surfaces. Quartz veins display a strong lineation, defined by elongate grains oriented parallel to the mylonite lineation. In granite gneiss mylonites, centimetre-spaced, sinistral S–C' fabrics (e.g. Fig. 4a) increase in frequency towards the central fault core trace of the HSF. Similar

asymmetric sinistral fabrics are seen in psammites (e.g. Fig. 4c) phyllonites and sheared pegmatites, but not in marble mylonites.

Throughout the HSFZ, the mylonites preserve millimetre- to centimetre-scale close to isoclinal folds of quartz veins, pegmatites and diorite sheets with markedly curvilinear fold hinges (Fig. 4b). The fold-hinge orientations lie along a girdle subparallel to the mean steeply dipping ENE–WSW axial plane and the mylonite foliation (Fig. 5, fourth row down). Where steeply plunging, folds show a consistent sinistral sense of vergence (Fig. 4b). Centimetre-scale 'eye' structures are widespread and suggest that sheath folding (Cobbold and Quinquis 1980) has occurred synchronous with sinistral shear. At distances of less than 200 m of the central fault core, S–C' fabrics are folded by centimetre-scale, open to close, steeply plunging sinistral folds with rounded hinge zones. Steeply dipping, centimetre- to millimetre-scale kink bands with angular hinges overprint the mylonitic foliation (Fig. 5, fourth row down). These display predominantly sinistral vergence (trending east–west to ESE–WNW), but a subordinate set of NE–SW dextral kink bands

Hitra-Snåsa Fault

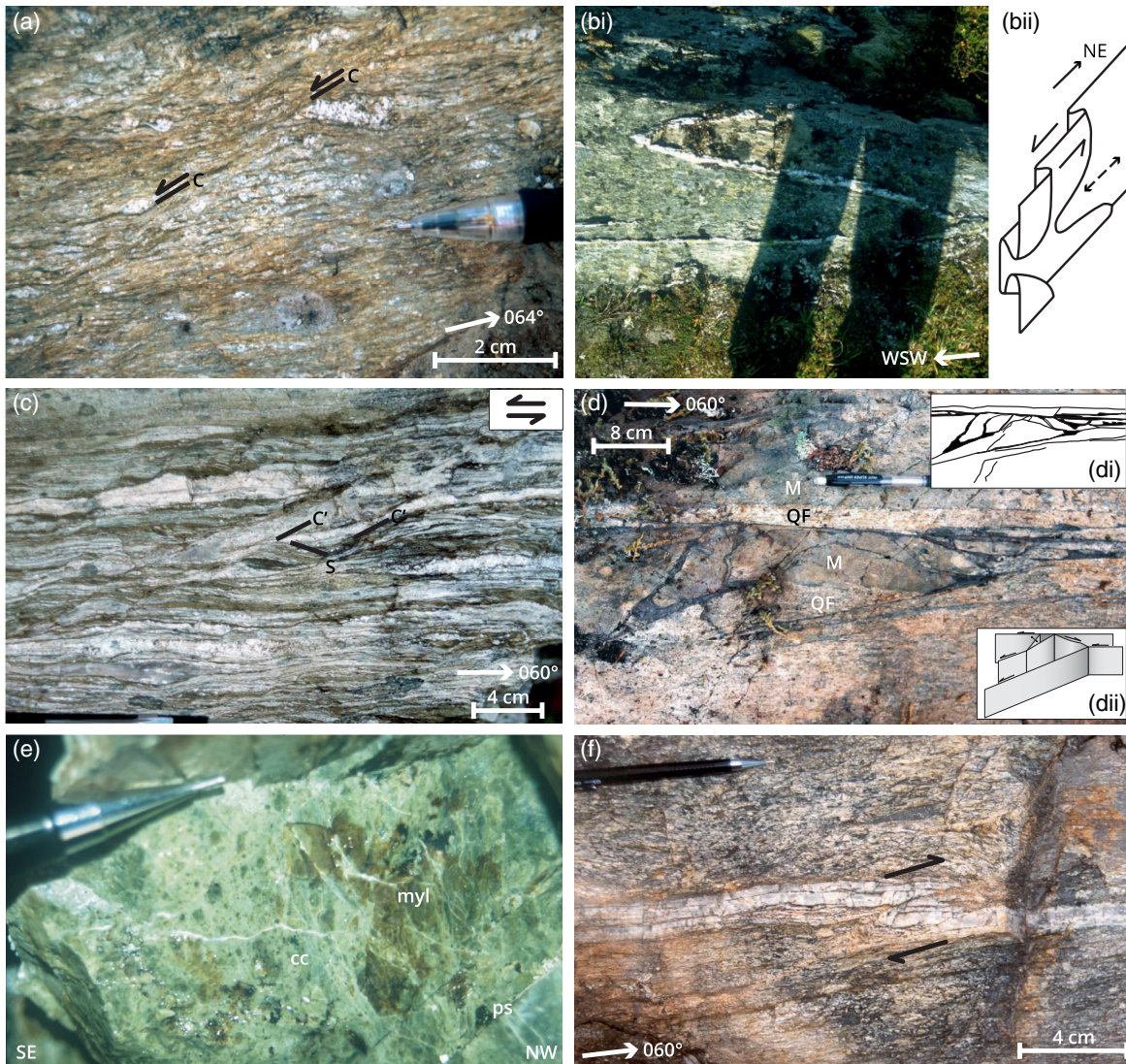


Fig. 4. Plan views of fault rocks and structures from the HSFZ of the Mefjellet area (unless indicated otherwise). (a) Typical mylonite with S–C fabrics consistent with sinistral shear. (b) (i) Steeply plunging, sinistrally verging folded quartz vein, with (ii) 3D diagram summarizing inferred sheath-fold geometry for these structures relative to the subhorizontal mineral lineation (double arrow). (c) Mylonitized psammite with sinistral S–C fabrics, Follavetnet (for location see Fig. 1c, labelled H3). (d) Linked network of pseudotachylite-bearing faults and injection veins consistent with sinistral shear cutting mylonitized quartzo-feldspathic gneiss (QF) and mafic intrusions (M). Inset (i) shows summary sketch of (d), with inset (ii) showing a 3D fault plane interpretation. (e) Typical green cataclasite from the core of the HSFZ with randomly oriented clasts of earlier mylonite (myl), cataclasite (cc) and pseudotachylite (ps). The cataclasite here is cross-cut by undeformed pale calcite veins. (f) NE–SW fault dextrally offsetting mylonitized quartz vein.

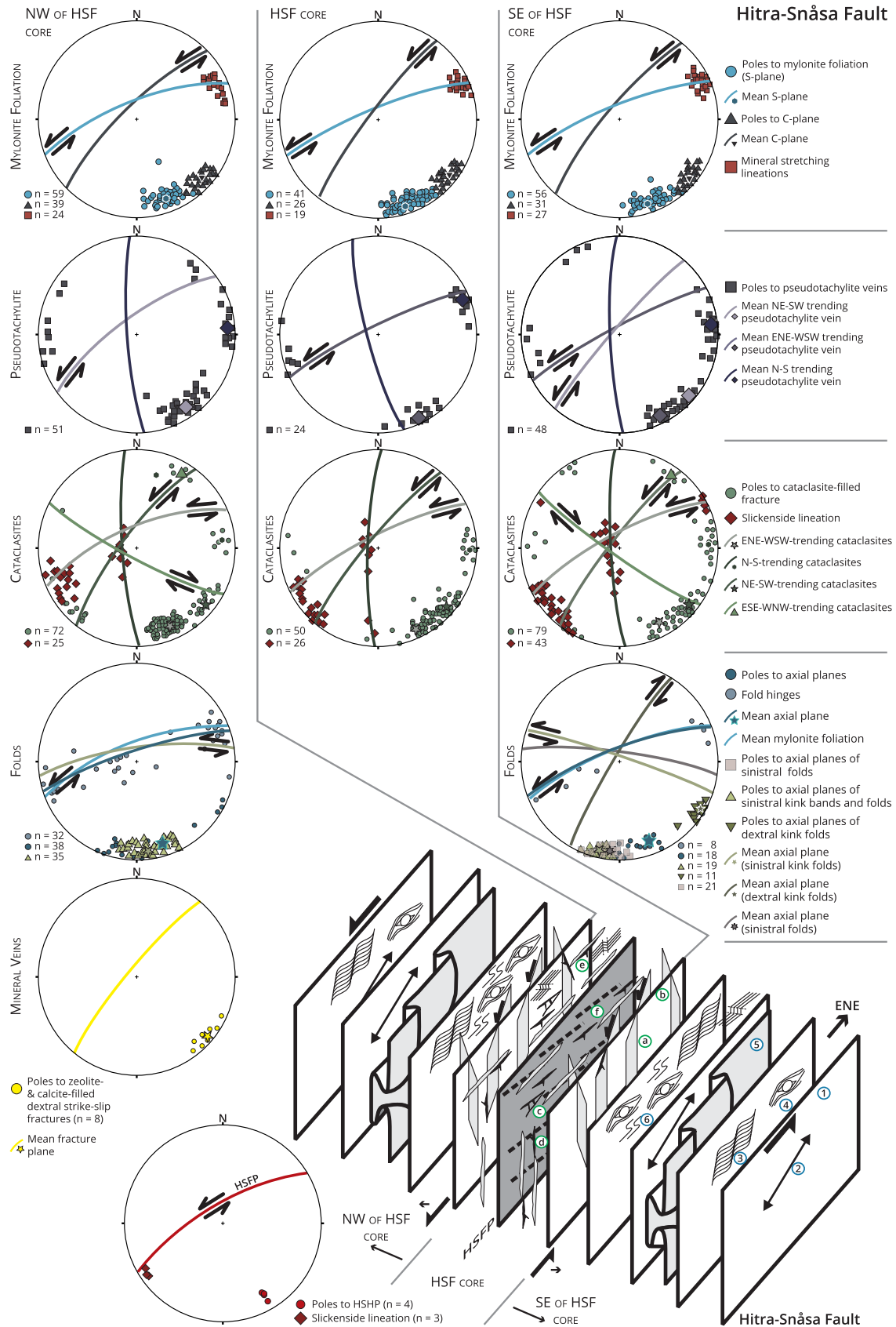


Fig. 5. Labeled stereonet of structural data from NW (left column) and SE (right column) of the HSFZ core (centre column) in the Mefjellet area. All are equal area lower hemisphere plots. Bottom right shows 3D summary of ductile (numbers) and overprinting brittle structures (letters) formed during first two deformation events along the HSFZ, Mefjellet area. Lowermost stereonet shows orientation of exposed Hitra-Snåsa fault plane (HSFP) and associated slickenlines. 1, Subvertical foliation; 2, mineral stretching lineation; 3, sinistral S-C' fabrics (millimetre- to centimetre-scale); 4, σ -type porphyroclasts (sinistral, millimetre- to centimetre-scale); 5, sheath folds (metre-scale) and sinistral vergence; 6, S-C' fabrics refolded by steeply plunging sinistral verging folds (centimetre-scale). a, R-type Riedel shears filled with cataclasite and/or pseudotachylite; b, extensional faults filled with cataclasite and/or pseudotachylite; c, foliation-parallel brittle faults containing centimetre-thick cataclasite; d, centimetre-scale pseudotachylites; e, sinistral and dextral verging kink bands; f, slickenside lineations on HSFP.

are found SE of the fault core and are interpreted to represent local conjugate structures.

Brittle damage zone. Thin pseudotachylite veins (e.g. Fig. 4d) have been recognized up to 280 m on either side of the central fault core but are less well developed on the southeastern side. Centimetre-thick veins are common at distances of less than 70 m from the core. The near-vertical pseudotachylites trend NE–SW to ENE–WSW and north–south (Fig. 5, second row down). All overprint and locally reactivate the pre-existing mylonitic foliation. They commonly occur adjacent to well-defined narrow slip surfaces and pass into a marginal cataclasite adjacent to the mylonitic host rock. Many pseudotachylites form networks bound by parallel pairs of ENE–WSW- to NE–SW-trending slip surfaces. Discordant NNW–SSE- to north–south-trending injection veins nucleate off these bounding slip surfaces and commonly lie in an echelon arrangements consistent with sinistral shear (e.g. Fig. 4d). Many ENE–WSW- to NE–SW-trending pseudotachylites link into R-type Riedel shears filled with thin pseudotachylite or cataclasite that sinistrally offset the mylonite foliation by up to 10 cm. Elsewhere, injection veins overprint Riedel shears, thus suggesting that there were multiple melting events during the sinistral movements.

At distances of less than 50 m from the central fault core, foliation-parallel (ENE–WSW) faults containing centimetre-thick cataclasites (e.g. Fig. 4e) branch into networks of subvertical fractures. The cataclasite-filled fractures form three main clusters: ENE–WSW to NE–SW, north–south and WNW–ESE. ENE–WSW- to NE–SW-striking fractures carry subhorizontal slickenside lineations and display sinistral strike-slip offsets of 5–30 cm (Fig. 5, third row down). These fractures are interpreted as R-type Riedel shears. North–south-trending extensional fractures with sporadic dip-slip quartz slickenfibres link into ENE–WSW master faults. NE–SW-trending fractures with subhorizontal slickenside lineations offset the mylonite foliation and quartz veins by 2 cm to 2 m in a sinistral sense and link into the same ENE–WSW-trending structures. The NE–SW-trending fractures are interpreted as R-type Riedel shears. Less widespread ESE–WNW-oriented fractures are found in rocks immediately SE of the fault core with subhorizontal slickenside lineations displaying dextral strike-slip offsets of 1–5 cm. They are interpreted as R'-type Riedel shears. Collectively, all the various brittle fractures are consistent with sinistral shear along the HSFZ.

In several locations NW of the fault core, small NE–SW-oriented subvertical fractures offset the mylonite foliation by 1–5 cm in a dextral sense (Fig. 4f). The fractures are associated with centimetre-scale kink bands located near the tip zones of the fractures, which display a dextral sense of vergence. The fractures contain subhorizontal slickenside lineations and millimetre-thick zeolite and calcite veins. The zeolite and calcite veins fill subvertical fractures trending NW–SE, which display small dextral strike-slip offsets. It is unclear whether these fractures represent a later dextral reactivation or are related to the dextral kink bands seen SE of the fault core that were then passively filled by later zeolite and calcite mineralization. The zeolite- and calcite-filled fractures are also associated with NNE–SSW-oriented fractures, which display sinistral strike-slip offsets of 1–2 cm.

Brittle fault core. The 20 m-wide HSFZ fault core is well exposed at map reference 32V NR 7796 8719 (Fig. 3b) where intensely fractured quartzo-feldspathic mylonites are overprinted by 2–40 cm-thick breccia zones bounded by centimetre-thick, epidote-rich cataclasites trending ENE–WSW. These are spaced 3 cm to 2 m apart towards the outer parts of the core and increase in frequency towards the fault core by an order of magnitude. Slickenlines, where exposed on steeply NNW-dipping polished fault surfaces, plunge shallowly WSW (Fig. 5, third row down). Millimetre- to centimetre-

thick pseudotachylite veins are widespread, localizing along the ENE–WSW-trending mylonite foliation and linking into north–south tensional or extensional structures with dip-slip slickenlines (Fig. 3b). Pseudotachylite veins both cross-cut and are present as clasts within the cataclasite matrix, suggesting that cataclasite and pseudotachylite development was coeval. Minor zeolite veins (millimetre-thick) localize along and transect the epidote-rich cataclasites and offset them by 1–5 cm in an apparent dextral sense.

Summary. At least three phases of deformation are recognized associated with the steeply dipping HSFZ. During the earliest event, a >1 km-wide ductile shear zone with mylonites deforms the banded gneiss country rocks and has been dated by Sherlock *et al.* (2004) at 406 ± 11 Ma using Ar–Ar infrared laser ablation of syntectonic muscovite growths. Shallowly plunging mineral stretching lineations, ductile sheath folds, S–C fabrics and conjugate kink bands are all associated with this ductile shear zone and are consistent with sinistral shear (Fig. 5, 3D diagram). The occurrence of pegmatite and microdiorite dykes, and extensive quartz veining, all of which predate mylonitization, increase in frequency towards the centre of the HSFZ, and may indicate the presence of a precursor deep-seated basement structure; the dykes are not found outside the HSFZ within the banded gneisses.

Later brittle reactivation of the HSFZ led to the development of overprinting, foliation-parallel and cross-cutting cataclasites and pseudotachylites, together with the formation of west-dipping, north–south-trending extensional faults, which link into the HSF plane, and other subparallel structures (Fig. 5, 3D diagram). The abundance of these extensional faults, which link into sinistral strike-slip, ENE–WSW-oriented faults, is consistent with sinistral transtension. Pseudotachylites that formed during these movements have been dated at 290 ± 10 Ma (Sherlock *et al.* 2004). Finally, later small centimetre-scale dextral strike-slip offsets are associated with millimetre-thick zeolite mineralization infills of pre-existing NE–SW- to ESE–WNW-trending subvertical fractures.

The Verran Fault Zone

The Verran Fault Zone (VFZ) refers to a zone of rocks that are deformed owing to movements along large NE–SW-trending structures such as the Verran Fault (VF) and Elvdal Fault (EF), and shorter north–south- or NNE–SSW-linking faults such as the Raudtindalen Fault (RF) (Fig. 1b and c). The main exposures lie to the north of Verrasundet and in a series of stream or road sections along Skaudalen to the SW of Verrasundet. Lineament interpretations from Landsat™ images by Grønlie and Roberts (1989) combined with analysis of aerial photographs and geological maps revealed a complex array of anastomosing faults initially interpreted to be consistent with earlier sinistral and later dextral strike-slip movements.

Shear-zone mylonites. Mylonites and protomylonites are poorly preserved along the entire length of the VFZ and are best exposed in the Skaudalen stream section (Fig. 1c). Here, mylonitic rocks derived from porphyritic granite display a well-developed foliation defined by flattened and stretched aggregates of quartz, mica and feldspar (Fig. 6ai) with lineations defined by elongate quartz, mica and feldspar grains. The mylonite foliation trends ENE–WSW and dips steeply SE, with lineations plunging shallowly ENE (Fig. 6aai). In outcrop surfaces viewed normal to the foliation and parallel to the lineation, feldspar porphyroclasts (up to 3 cm in length) display σ - and δ -type geometries consistent with sinistral shear (Fig. 6ai). In thin-sections, millimetre-scale S–C' fabrics are also consistent with sinistral shear. The mylonites here are cross-cut by NNE–SSW-trending, centimetre-thick, steeply dipping, brick-red to orange-coloured zeolite and calcite-cemented fault breccias with

subhorizontal slickenfibres and marginal drag folds consistent with sinistral displacements (Fig. 6a_{iii}). These are interpreted to represent R' shears associated with later dextral shear along the VFZ (Fig. 6a_{iv}).

Brittle damage zone. Three representative sections are summarized here that expose different parts of the VFZ; other localities have been described in detail by Watts (2001).

(1) Outer VFZ damage zone, Ormsetvatnet and hydro station road sections. The faults here overprint the steeply SSE-dipping gneissose foliation and associated shallowly ENE-plunging mineral lineation (Fig. 6b_i). Earlier ENE–WSW- and NNE–SSW-trending, steeply dipping fractures are lined with green cataclasite and are consistently cross-cut by brightly coloured (white, grey, orange) zeolite and calcite mineralization and veins (Fig. 6b_{ii} and b_{iii}). Fault-related deformation first appears c. 500 m NW of the Verran Fault plane (VFP) trace forming metre-thick, high-strain zones (intense fracturing) that are separated from metre-thick low-strain zones across ENE–WSW-trending, SE-dipping fracture surfaces localized along the pre-existing gneissose foliation. Millimetre-thick, NNE–SSW-trending cataclasites with subhorizontal slickenside lineations link into foliation-parallel fractures. The cataclasites locally offset the gneissose foliation by up to 2 m in a sinistral sense and are interpreted as R-type Riedel shears formed during sinistral strike-slip movements along the VFZ.

At a distance of 450 m NW of the VFP trace, 1–50 cm-thick zeolite breccias are exposed. These are spaced from 4 to 15 m apart and are localized along the ENE–WSW-trending gneissose foliation. Most breccias are bounded by slickenfibres-covered fault planes, which indicate both dip-slip normal and dextral strike-slip movements, based on calcite and zeolite fibre stepping. Dip-slip normal slickenfibres are consistently overprinted by dextral strike-slip slickenfibres (Fig. 6b_{iv}). ESE–WNW-trending zeolite and calcite veins (0.5–1 cm thick, shown in Fig. 6b_{ii}) with subhorizontal slickenside lineations offset pre-existing cataclasites by up to 4 cm in a dextral sense. Tensional calcite and zeolite veins (1 mm to 1 cm) link into the ESE–WNW-oriented veins and trend NNW–SSE, displaying an echelon geometries.

The NE–SW-trending dip-slip zeolite- and calcite-mineralized faults, and a set of subordinate north–south-trending structures, are notably well exposed in a 60 m-long road section close to the hydro station (map reference 32V NR 8350 8115; Fig. 1c). These overprint earlier green cataclasites and display widespread dip-slip slickenfibres with stepping patterns consistent with normal fault movements (Fig. 6b_v).

In summary, the outer parts of the VFZ contain mainly foliation-parallel cataclasites formed during sinistral strike-slip movements, overprinted by zeolite- and calcite-mineralized breccias and veins. The breccias are associated with dip-slip normal (SE-side down) faults that were locally reactivated during a slightly later phase of dextral strike-slip movement.

(2) Inner VFZ damage zone, Verrabotn stream section and Verrasundet shoreline. All the fault rocks exposed along these sections are lithologically and texturally similar and overprint banded granodioritic gneisses (Fig. 7a–f). The foliations dip steeply to the SE with shallowly plunging mineral lineations in both locations (Fig. 7b_i and e_i). The cataclastic deformation is most intense closer to the ENE–WSW-trending VFP trace, which lies just offshore in Verrasundet.

Unfoliated pale green cataclasites are the earliest fault rocks recognized. These range from 1 mm to several metres in thickness and form anastomosing geometries around less deformed areas of granodiorite gneiss (Fig. 7a and d). Two main clusters are recognized: NE–SW-striking, SE-dipping and north–south-trending, dipping steeply east and west (Fig. 7b_{ii} and e_{ii}). NE–SW-trending cataclasites appear to localize along the pre-existing gneissose

foliation (Fig. 7a and d) and display subhorizontal slickenfibres of quartz and epidote, and secondary NNE–SSW Riedel shears that indicate sinistral strike-slip movements (Fig. 7c). North–south-striking cataclasites link into the NE–SW-trending structures and display dip-slip normal slickenfibres. The north–south-trending cataclasites are interpreted as extensional faults formed during sinistral transtension along the ENE–WSW-trending VFZ.

Zeolite- and calcite-mineralized breccias everywhere overprint earlier formed cataclasites (Fig. 7a and d). The breccias are up to 1 m thick, are spaced 1–3 m apart and are bounded by discrete polished fault planes, which are commonly covered in slickenside and slickenfibres lineations. The breccias occur in a range of steeply dipping orientations, striking north–south clockwise to ESE–WNW (Fig. 7b_{iii} and e_{ii}). Many breccias localize along the ENE–WSW-oriented gneissose foliation and the pre-existing ENE–WSW- and north–south-trending cataclasites (Fig. 7a and d). Slickenside lineations show a large scatter. ENE–WSW-trending breccias display evidence of dip-slip normal movements that are consistently overprinted by dextral strike-slip to oblique movements based upon the stepping direction of zeolite and calcite fibres. North–south-trending breccia slickenfibres indicate sinistral strike-slip movements, and are interpreted as R'-type Riedel shears formed during dextral strike-slip movements along the ENE–WSW-trending VFZ. The breccias are locally overprinted by later, randomly oriented, centimetre- to millimetre-thick calcite and zeolite veins.

In the Verrabotn stream section, zeolite- and calcite-mineralized breccias are cross-cut by soft grey gouges that trend NE–SW and dip mainly SE, with subhorizontal lineations defined by aligned clay particles. They are 1 mm to 10 cm thick and commonly form braided geometries. Gouges up to 50 cm thick are also well exposed in the nearby 720 road section where they display dextral shear bands and strike-slip offsets of 30 cm to 100 m (Watts 2001).

In summary, the inner part of the VFZ comprises a series of anastomosing cataclasite-bearing faults formed during sinistral shear that are overprinted by intense veining associated with the development of zeolite- and calcite-mineralized breccias. These breccias were formed during a phase of dip-slip normal movement (SE side down) along the VFZ closely followed by a phase of dextral strike-slip faulting. The breccias are overprinted by anastomosing grey fault gouges, formed during a later phase of dextral strike-slip movement.

(3) A NNE–SSW linking structure, the Raudtinddalen Fault. The Raudtinddalen Fault (RF) is a NNE–SSW-trending fault that dips steeply to the west and appears to link into the VFZ. It is well exposed in a steep-sided stream gorge NW of Verrasundet (Fig. 1c). Complex brittle faults and fractures associated with extensive green cataclasites, zeolite-cemented breccias and later zeolite and calcite veins are exposed and were first described by Grønlie *et al.* (1991).

At map reference 32V NR 7946 78723, a sharp, polished, fault plane (008/81W) separates fractured gneisses from a 20 cm-thick unit of green ultracataclasite forming the western margin of an 8 m-wide brittle deformation zone (Fig. 8a). The ultracataclasite is overprinted to the east by a 30 cm-thick zeolite- and calcite-mineralized gouge, which contains clasts of gneiss and earlier formed cataclasite. The mineralized gouge is cut by a series of randomly oriented, pale pink, zeolite veins (1 mm to 1 cm thick; laumontite according to XRD analyses by Grønlie *et al.* 1991). Both are then cross-cut by orange-coloured zeolite (stilbite; Grønlie *et al.* 1991) and calcite veins (1 mm to 1 cm thick). Farther east, a 1.2 m-wide zone of pale green cataclasite overprints granodiorite gneiss. Millimetre- to centimetre-thick zeolite and calcite veins cross-cut the cataclasite (Fig. 8a and b_i).

The cataclasite grades eastwards into a 5 m-wide zone of intensely fractured gneiss (locally brecciated) that is cut by a series of millimetre- to centimetre-thick braided cataclasites. Millimetre-thick zeolite and calcite veins overprint both the

Verran Fault: Outer damage zone

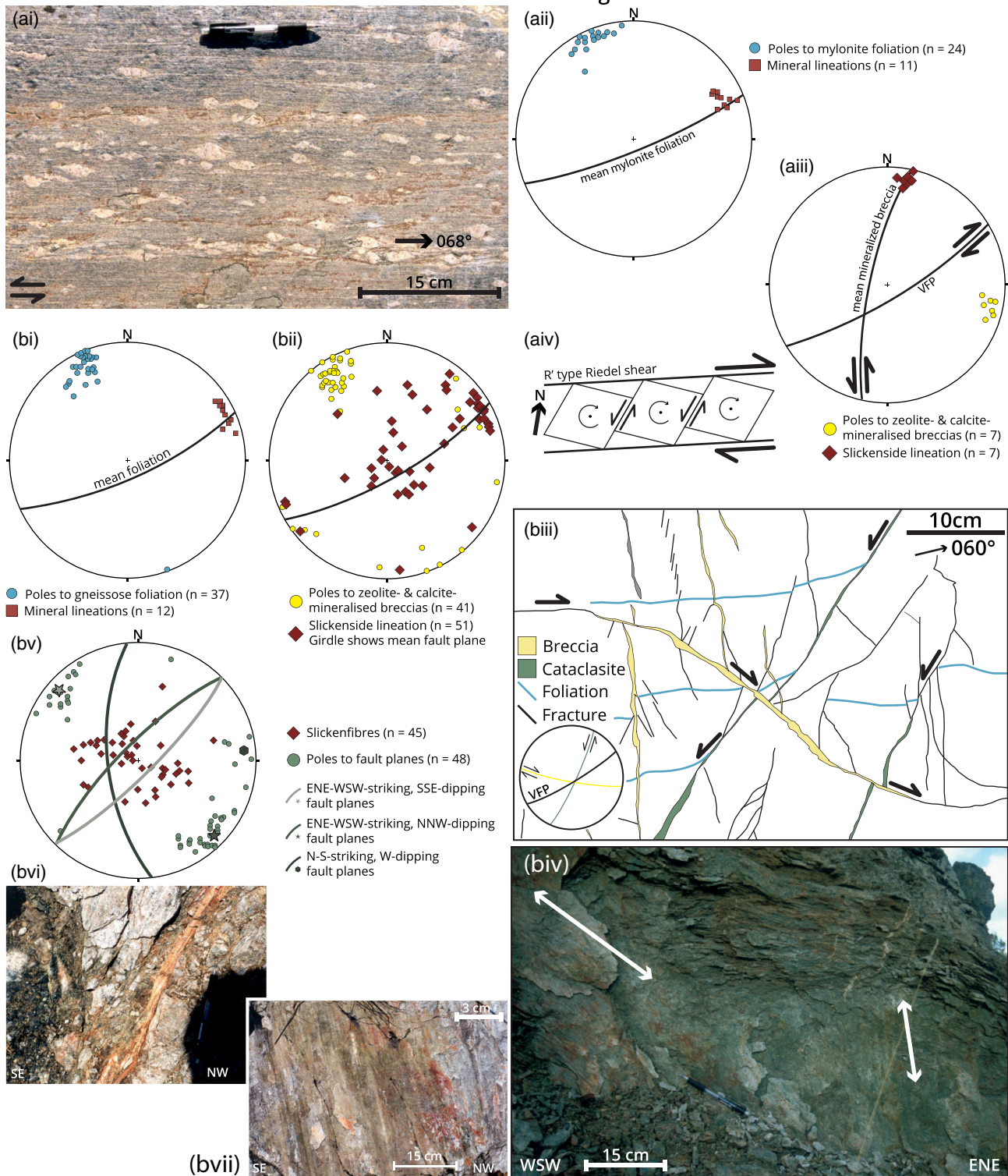


Fig. 6. (a) Structures associated with sinistral mylonites of the VFZ outer damage zone at Skaudalen (map reference 32V NR 6183 6217). (i) Plan view of mylonitized granitoid with σ feldspar porphyroclasts consistent with sinistral shear sense. (ii) Stereonet showing poles to mylonitic foliation and lineations. (iii) Stereonet showing poles to later zeolite- and calcite-mineralized breccia zones and associated slickenfibres relative to mean Verran Fault plane (VFP) orientation. (iv) Simple plan view summary of the suggested relationship between antithetic sinistral faults and dextral shear along the VFZ. (b) Structures associated with brittle deformation in the outer damage zone of the VFZ. (i) Stereonets of poles to gneissose foliation and stretching lineations. (ii) Stereonet showing poles to zeolite- and calcite-mineralized breccias and associated slickenfibres. (iii) Plan view of cross-cutting relationships between fault rocks and fabrics with summary stereonet in inset. (iv) Oblique view of exposed ENE-WSW-trending, SSE-dipping, fault surface with dip-slip slickenfibres overprinted by oblique dextral slickenfibres. In (b), parts (i)–(iv) are from Ormsetvatnet road section (for location see Fig. 1c). (v) Stereonet showing poles to zeolite- and calcite-mineralized breccias along faults and associated slickenfibres. (vi) Oblique view of dip-slip normal zeolite and calcite slickenfibres on exposed SE-dipping fault plane (note pen in shadow for scale). (vii) Oblique view of a north-south-oriented calcite-zeolite mineralized fault zone. Material in (v)–(vii) is from the Hydro Station locality (map reference 32V NR 8350 8115; for location see Fig. 1c).

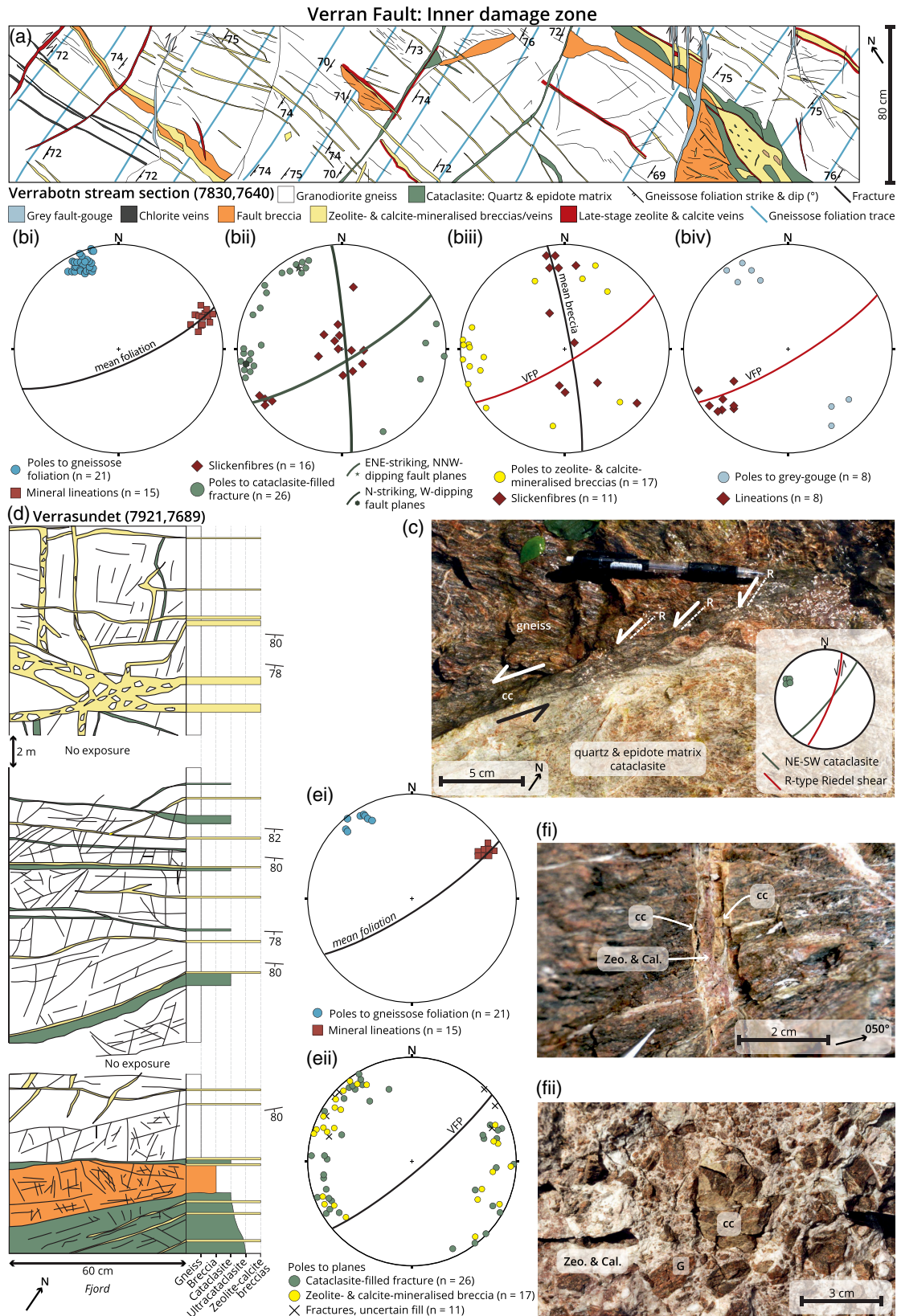


Fig. 7. Fault rocks and structures from the inner damage zone of the VFZ. (a) Structural log of the Verrabotn stream section (map reference 32V NR 7830 7640). (b) Stereonets of structures from the Verrabotn stream section. (i) Poles to foliation and mineral lineations in gneisses. (ii) Poles to cataclasites showing two main trends as great circles and associated slickenlines. (iii) Poles to zeolite- and calcite-mineralized breccias showing mean Verran Fault Plane (VFP) and mean breccia as great circles and associated slickenfibres. (iv) Poles to grey gouge-bearing faults and associated slickenline lineations, with mean VFP shown as great circle. (c) Plan view of NE-SW-trending, subvertical cataclasite exposed in stream section (cc) linked by sinistral R fractures; split arrows give inferred sense of shear along the cc-bearing fault. (d) Structural log of the Verrasundet stream section (map reference 32V NR 7921 7689). (e) Stereonets of structures from the Verrasundet section. (i) Poles to foliation and mineral lineations in gneisses. (ii) Poles to cataclasite and zeolite- and calcite-mineralized breccias showing mean VFP great circle. (f) (i) Plan view of north-south cataclasite (cc) reopened by multiple phases of later zeolite and calcite mineralization (Zeo and Cal.). (ii) Plan view of zeolite and calcite-mineralized breccia with fragments of gneiss (G) cut by earlier cataclasite (cc). Both images from Verrasundet section.

cataclasite and the fractured gneiss. Farther east, the gneiss is bounded by a 2 cm-thick zeolite- and calcite-mineralized gouge, which is overprinted eastwards by a 40 cm-thick zeolite- and calcite-mineralized breccia (Fig. 8a). This contains clasts of cataclasite and zeolite- and calcite-mineralized gouge (Fig. 8bii), suggesting that the zeolite- and calcite-mineralized breccia is the youngest fault rock.

In the well-exposed wall rocks immediately to the west of the RF, cataclasite-filled faults (shown in green in Fig. 8ci) display ENE–WSW-trending braided geometries that run subparallel to the pre-existing gneissose foliation (Fig. 8cii and ciii). These fault zones appear to connect into the core of the RF. They carry subhorizontal slickenfibres, which indicate sinistral strike-slip movements based upon the stepping directions of the quartz fibres and are thought to be R-type shears related to sinistral displacements along the VFZ. Zeolite- and calcite-mineralized breccias (shown in yellow in Fig. 8ci) appear to both cross-cut and develop along the earlier formed cataclasite and gneissose foliation. The breccias are bounded by discrete fault planes that form three main clusters: ENE–WSW-trending, dipping steeply SE; ENE–WSW-trending, dipping steeply NW; and east–west to ESE–WNW, dipping variably NNE (Fig. 8civ). The faults are spaced every 10 cm to 5 m and display a braided geometry surrounding slivers of intensely fractured gneiss. Zeolite and calcite slickenfibres form two main clusters: dip-slip and shallowly ENE plunging (Fig. 8civ). Dip-slip slickenfibres are consistently overprinted by dextral strike-slip slickenfibres along the ENE–WSW-trending faults.

Along the western side of the RF, the steeply west-dipping RF plane contains quartz slickenfibres indicating dip-slip normal movements (Fig. 8a). Some 20 cm to the east, the ultracataclasite is separated from adjacent zeolite- and calcite-mineralized gouges by a subvertical north–south fault, which displays subhorizontal slickenside lineations (Fig. 8a). Still farther east, a 2 cm-thick zeolite-mineralized gouge is separated from the 40 cm-thick, zeolite- and calcite-mineralized breccia by a fault plane oriented 019/90 (Fig. 8a). The fault plane contains zeolite and calcite slickenfibres, which indicate sinistral strike-slip movement based upon the stepping direction of the mineral fibres.

In summary, the NNE–SSW-trending, steeply west-dipping RF and associated cataclasites or ultracataclasites appear to have initiated as an extensional fault during sinistral shearing along the nearby VFZ. Extensive later zeolite and calcite mineralization occurred during sinistral strike-slip reactivation of the RF, which is interpreted to have acted as an antithetic R'-type Riedel shear during dextral strike-slip reactivation of the VFZ. Although these faults were not ideally oriented for antithetic movement during dextral strike-slip along the MTFC, it is suggested that it was easier to reactivate these structures sinistrally rather than forming new, more optimally oriented structures.

Brittle fault core. The only exposures of the VF fault core are found in a stream section along Tangstadelva SW of Verrasundet (Figs 1c and 9; map reference 32V NR 7400 7320). Elsewhere, the core is eroded, submerged beneath the fjords (Verrasundet and Beitstadjord) or concealed under the thick Quaternary glacial deposits that fill the ENE–WSW-oriented valleys. The VFP here is oriented 058/86SE and lies within a 4 m-wide fault zone flanked by wall rocks on either side (Fig. 9).

NW of the VFP, intensely fractured granodiorite gneiss is overprinted by millimetre- to centimetre-thick foliated cataclasites (Fig. 9a and b). To the SE, this grades into a 50 cm-thick, epidote-rich cataclasite, which is cut by millimetre-scale quartz, epidote and chlorite veining. The cataclasite contains no fabric and appears to be isotropic. In places, it contains millimetre-thick, ENE–WSW-trending, dark brown to black, indurated gouges that define a crude banding in the field. Farther to the SE, the cataclasite is cut by a

more substantial 5 cm-thick, brown to black, indurated fault gouge (Fig. 9a, b and ci). The contact is irregular and the gouge displays millimetre- to centimetre-scale, north–south injection veins that cross-cut the epidote-rich cataclasite.

The indurated fault gouge contains clasts of cataclasite, suggesting that it is the younger fault rock. The contact between the indurated fault and the soft grey gouge to the SE is sharp and polished (059/80SE). The soft grey gouge contains fragments of earlier formed cataclasite, indurated gouge and zeolite- or calcite-mineralized breccia (Fig. 9b) suggesting that the gouge is younger than these fault rocks. The grey gouge is at least 15 cm thick and to the SE it grades into an incohesive breccia zone that is *c.* 1.5 m thick (Fig. 9a and b). The incohesive breccia sporadically crops out along the Tangstadelva stream bed and contains fragments of earlier formed cataclasite, indurated gouge and mineralized (zeolite and calcite) breccia. Centimetre-thick grey gouges cross-cut the incohesive breccia and display ENE–WSW anastomosing geometries. On the SE side of the stream, the incohesive breccia grades into a 30 cm-thick grey gouge. Here, the grey gouge (Fig. 9bii and ciii) contains fragments (up to 30 cm in length) of gneiss and zeolite- and calcite-mineralized breccia, suggesting that the grey gouge is younger than these fault rocks. Within the centre of the grey gouge, a 5 cm-thick, blue–grey gouge (Fig. 9civ) transects the grey gouge and is interpreted to be the youngest fault rock within the VF core, corresponding to the VFP (058/86SE) (Fig. 9bi). To the SE of the gouges, a 25 cm-thick zeolite and calcite breccia (Fig. 9bi and cii) is exposed. The breccia is cut by grey gouge to the NW and an incohesive breccia on its southeastern side (Fig. 9bi). The incohesive breccia overprints and grades into intensely fractured gneiss to the SE. Millimetre-thick cataclasites and pseudotachylites overprint the intensely fractured gneisses in the immediate wall rocks (Fig. 9bi).

ENE–WSW-trending, millimetre-thick cataclasites appear to localize along the pre-existing gneissose foliation both to the NW and to the SE of the VFP (Fig. 9di and dii). North–south- and NE–SW-trending cataclasites display braided geometries and commonly link into ENE–WSW-oriented cataclasites. The ENE–WSW- and NE–SW-trending cataclasites contain sparse subhorizontal slickenside lineations. In thin-sections viewed parallel to the slickenside lineations and normal to the ENE–WSW-striking and steeply dipping cataclasites, NE–SW-trending, chlorite-filled linking fractures display offsets of the gneissose foliation of up to 3 cm in a sinistral sense; these are therefore interpreted as R-type Riedel shears. The north–south-trending fractures display dip-slip slickenside lineations and kinematics consistent with extension. All of these cataclasite- and chlorite-bearing fractures are therefore interpreted to have formed during sinistral transtension along the ENE–WSW-trending VFZ. To the SE of the VFP the gneisses are overprinted by millimetre- to centimetre-thick, foliation-parallel pseudotachylites (Fig. 9bi) that display very sharp boundaries, injection vein geometries and usually bound a 2–5 cm-wide zone of brecciated gneiss. The pseudotachylites do not show any kinematic indicators in the field and are interpreted to be broadly coeval with the cataclasites seen in the fault core.

The brown–black indurated fault gouge contains an ENE–WSW-trending colour banding, which dips steeply to the SE (Fig. 9diii) and is defined by grain-size variations, compositional layers and the alignment of clasts. Subhorizontal quartz slickenfibres, which plunge shallowly to the WSW, indicate sinistral strike-slip movements based upon the stepping direction of the quartz mineral fibres. Backscatter SEM images show layers of Ca-smectite and pyrophyllite transected by sinistral-verging folds in polished blocks cut parallel to the slickenfibres lineations and normal to the foliation.

The 1.5 m-thick incohesive breccia contains slivers of calcite- and zeolite-mineralized breccia and fragments of cataclasite forming ENE–WSW-trending lenses that dip steeply to the SSE.

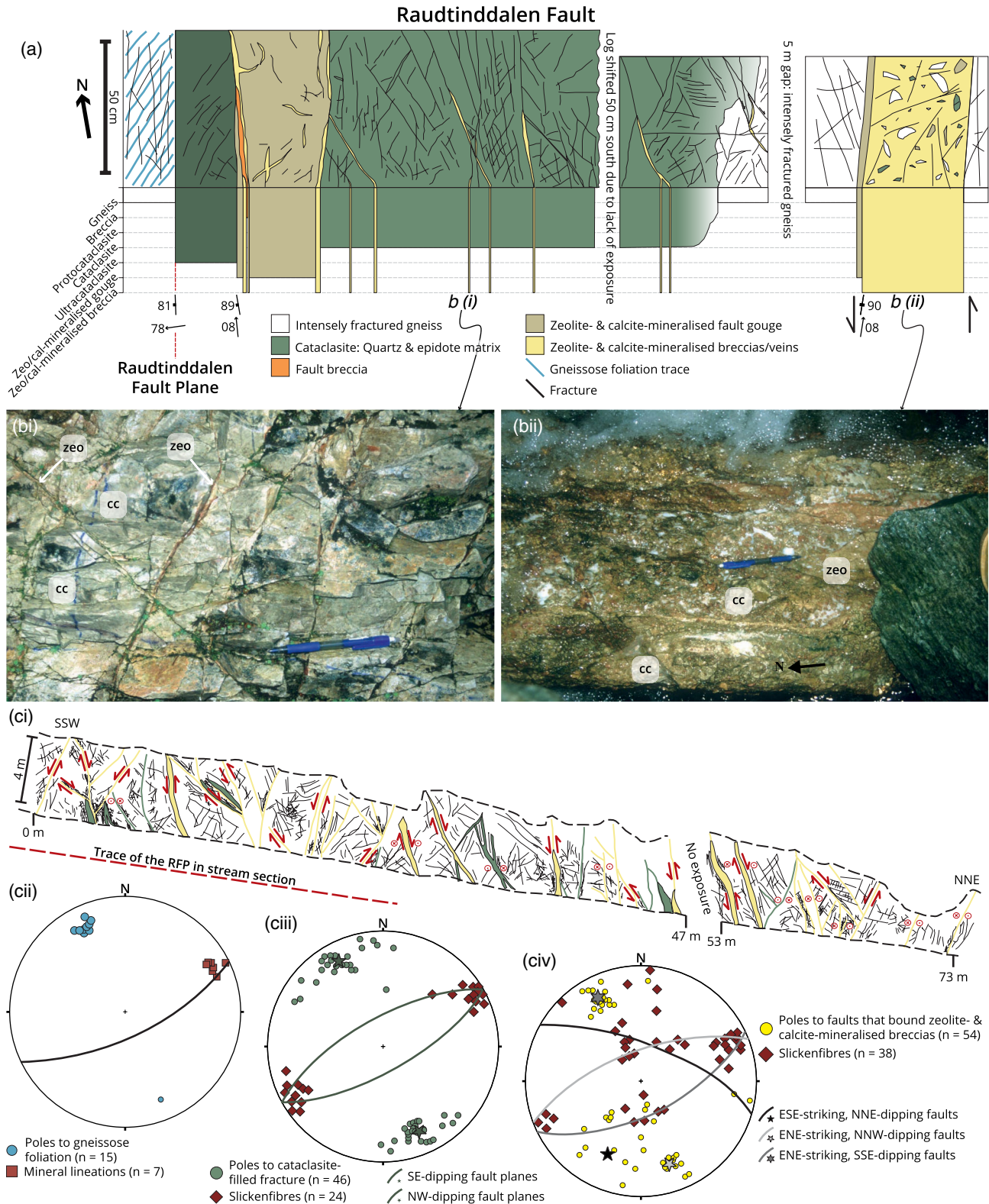


Fig. 8. Structures and fault rocks associated with the north–south Raudtinddalen Fault. (a) Structural log through the Raudtinddalen Fault core (map reference 32V NR 7946 7872). Locations of images shown in (b) are also indicated. (b) (i) Plan view of cataclasite (cc) cross-cut by network of calcite and zeolite veins (zeo). (ii) Plan view of zeolite- and calcite-mineralised breccias with clasts of earlier formed cataclasite (cc) and cross-cutting dark zeolite gouge (zeo). (c) (i) Sketch cross-section of rock wall exposed parallel to Raudtinddalen Fault Plane (RFP) with cataclasite- and calcite-zeolite-bearing fractures or faults shown in green and yellow, respectively. (ii) Poles to foliation, and mineral lineations in gneisses. (iii) Poles to cataclasites showing two main trends as great circles and associated slickenlines. (iv) Poles to zeolite- and calcite-mineralized breccias showing associated slickenfibres. (ii)–(iv) are from the section shown in (i).

SE-dipping surfaces of the mineralized breccias display dip-slip normal slickenfibres, which are consistently overprinted by dextral strike-slip slickenfibres (Fig. 9div).

To the SE, the incohesive breccia grades into a 30 cm-thick grey gouge with gneiss blocks that contains subhorizontal slickenline lineations (Fig. 9dv). NNE–SSW-trending, subvertical fractures

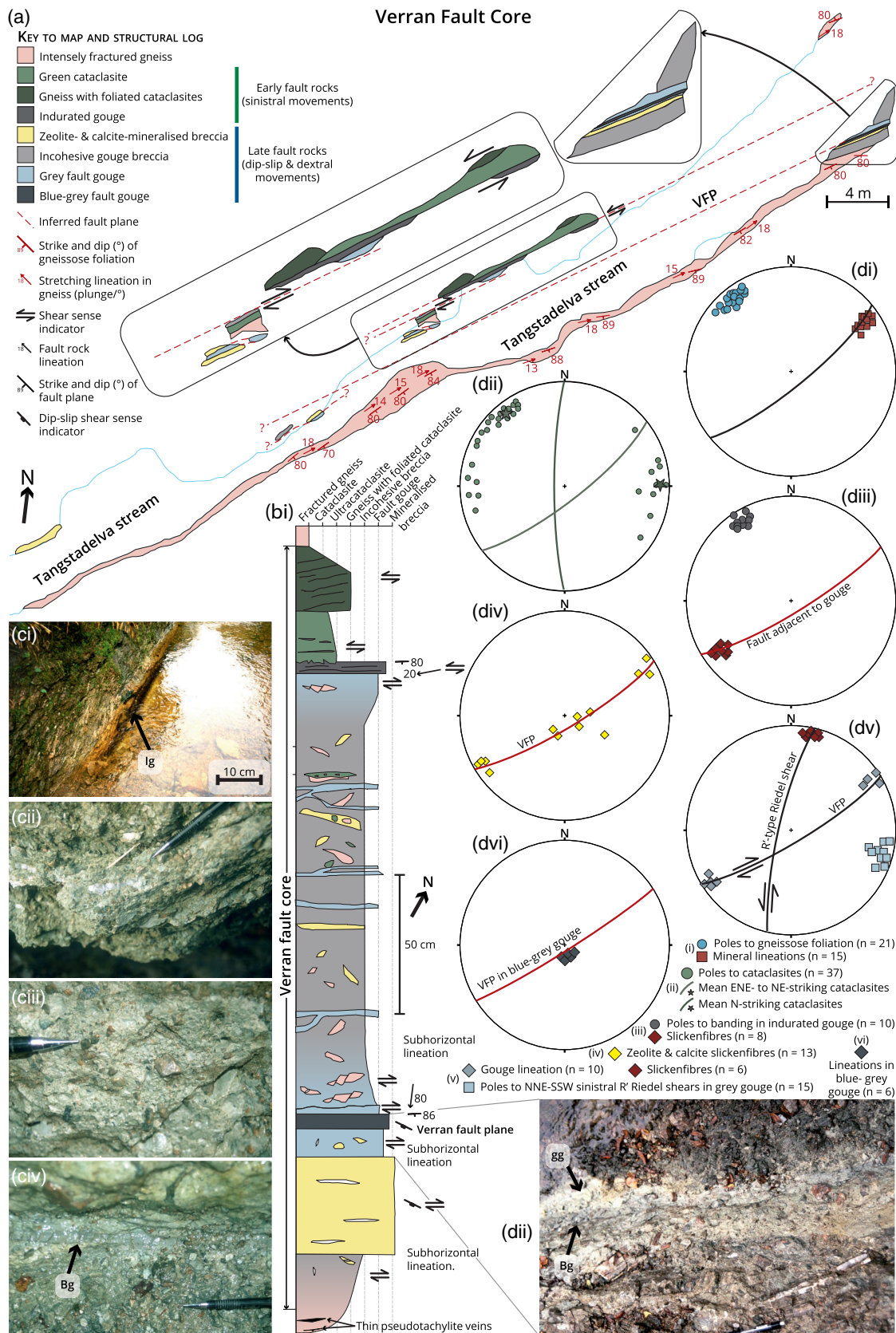


Fig. 9. (a) Detailed cairn map of the exposed Verran Fault core, Tangstadelva stream at map reference 32V NR 7400 7320, with critical sections shown in insets. (b) (i) Composite schematic log through Verran Fault core based on mapping shown in (a). (ii) Plan view of blue gouge (Bg) along Verran Fault Plane cutting grey gouge (gg). (c) Examples of fault rocks from the Verran Fault core. (i) Dark indurated fault gouge (lg). (ii) Zeolite- and calcite-mineralized breccia. (iii) Grey fault gouge. (iv) Blue-grey fault gouge (Bg). (d) (i) Stereonet showing poles to mylonitic foliation and lineations. Mean foliation is also shown as a great circle. (ii) Stereonet showing poles to cataclasites and two main trends shown as great circles. (iii) Stereonet showing poles to colour banding in indurated fault gouge and associated slickenfibres, with main associated fault plane shown as a great circle. (iv) Stereonet showing later zeolite and calcite slickenfibres relative to mean VFP orientation. (v) Stereonet showing poles to sinistral R' shears within grey gouge, with mean VFP and R' planes shown as great circles. Associated slickenline lineations also shown. (vi) Stereonet showing VFP as a great circle with associated slickenline lineations from blue-grey gouge.

with subhorizontal slickenside lineations (Fig. 9dv) offset the gneissose blocks by up to 30 cm in a sinistral sense. These fractures are interpreted as sinistral strike-slip, R'-type Riedel shears formed during dextral strike-slip movements along the VFZ. The thin (5 cm-thick), blue–grey gouge oriented at 058/86SE that cross-cuts the grey gouge represents the most recent movement phase along the VFP and carries a steeply SE-plunging slickenline lineation (80/158) (Fig. 9dvi).

Thus the fault rocks and structures within the VFZ core display evidence for at least four phases of reactivation through repeated localization along pre-existing structures and fault rocks. The earliest fault rocks are cataclasites, indurated fault gouges and pseudotachylites that are interpreted to have formed during sinistral movements along the VFZ (Fig. 9a). Zeolite- and calcite-mineralized breccias were formed during dip-slip normal faulting followed closely by a later phase of dextral strike-slip faulting forming anastomosing grey gouges surrounding zones of incohesive breccia. The most recent phase of movement is recorded by a thin blue–grey gouge, which localizes along the pre-existing grey gouge and was formed during a final phase of dip-slip movement.

Summary. The VFZ comprises a 0.5 km-wide zone of intense cataclastic deformation together with hydrothermal alteration and mineralization. At least five phases of movement are recognized (oldest to youngest), as follows.

- (1) Early rare mylonites formed during sinistral shearing and are correlated with the mylonites along the HSFZ, as they display similar overprinting relationships, textures and microstructures.
- (2) A more widespread assemblage of indurated cataclasites, fault gouges and minor pseudotachylite veins formed during sinistral brittle faulting along the ENE–WSW VFZ also leading to the formation of north–south-trending extensional faults such as the RF.
- (3) A third phase of reactivation involved dip-slip normal movements followed closely by dextral strike-slip movements along the VFZ, which led to the development of zeolite- and calcite-mineralized breccias and gouges. Linking north–south-trending faults (such as the RF) were reactivated as antithetic sinistral strike-slip shears.
- (4) All of the above fault rocks are consistently cross-cut by grey gouges associated with a later dextral strike-slip movement phase.
- (5) A blue–grey gouge developed along the VFP represents the most recent phase of movement and contains a well-defined dip-slip lineation. The sense of shear is unknown.

Fault-rock microstructures and evolution

The textural and mineralogical features of the predominant Banded Gneiss Complex protoliths and derived fault rocks are now summarized briefly in the order of their relative age (oldest to youngest). A more detailed account has been given by Watts (2001).

Protoliths

The overwhelmingly predominant quartzo-feldspathic banded gneisses of the Banded Gneiss Complex of Fosen typically comprise interlocking aggregates of equigranular feldspar (0.5–1 mm in size) interlayered with flattened, polygonal aggregates of quartz (0.5–1 mm in size), which surround isolated aggregate or grains of biotite, epidote and, more rarely, titanite and muscovite. The observed textures are typical of amphibolite-facies gneisses.

Mylonites

These are ubiquitous along the HSFZ, but texturally identical mylonites are found at only one locality associated with the VFZ (at Skaudalen; Figs 1c and 6a). They typically comprise feldspar porphyroclasts that are wrapped by a network of polycrystalline quartz ribbons and bands of fine-grained muscovite, chlorite and albitic plagioclase (Fig. 10a and b). Towards the centre of the HSFZ, with increasing strain, the mylonites are finer grained and contain higher proportions of chlorite and white mica compared with the coarser, lower-strain fault rocks. In addition, biotite is progressively replaced by fibrous chlorite.

The relative abundances of hydrous mineral phases (white mica, chlorite and epidote) suggest that retrograde metamorphism accompanied the mylonitization along the MTFC. The growth of chlorite and white mica synchronous with sinistral shear, and the coexistence of these minerals with fine-grained albite, probably indicates mid-greenschist-facies conditions (Yardley 1989). Polygonal quartz ribbons and muscovite display evidence for widespread, dynamic, subgrain rotation recrystallization whereas feldspar grains are relatively rigid and show brittle fracturing. Collectively, therefore, the mylonites along the HSFZ are considered likely to have formed in the temperature range 300–500°C, corresponding to depths of 10–15 km assuming an average geothermal gradient of 30°C km⁻¹.

Cataclasites

Texturally and mineralogically identical, pale green, cataclastic-series rocks are derived either from quartzo-feldspathic mylonites (HSFZ) or banded granitic gneisses (VFZ and RF). The cataclasites typically comprise finely comminuted clasts of wall rock, pseudotachylite (HSFZ and Verran fault core only), cataclasite, feldspar, quartz, chlorite, epidote, muscovite and titanite set within a fine-grained cataclastic matrix (Fig. 10c and d). The proportion of matrix varies from c. 10 to 90%. Randomly oriented clasts are poorly sorted, angular to subangular, ranging from 5 mm to less than 5 µm in size. Feldspar clasts are partially altered and are replaced by fine-grained aggregates of sericite and locally calcite. The cataclasite matrix is composed of inequigranular fragments (1–30 µm) with quartz and K-feldspar preserving overgrowths as a result of pressure solution, with evidence of redistribution of quartz and K-feldspar into voids and pore spaces.

The dominant deformation mechanisms are considered to be mechanical disaggregation and grain-size diminution (cataclastic flow), grain-boundary sliding and pressure solution. Quartz, feldspar and mica all deform by cataclasis, indicating temperatures of less than 250°C. Pressure solution has also occurred locally at grain contacts, leading to dissolution and precipitation of K-feldspar and quartz into voids and pore spaces. The cataclasites are inferred to have formed at temperatures between c. 200 and 250°C corresponding to depths of 6–8 km, assuming an average geothermal gradient of 30°C km⁻¹.

Pseudotachylites

The MTFC pseudotachylites are mostly found along the HSFZ and typically comprise randomly oriented, rounded to subrounded clasts (c. 30%) of feldspar, quartz, cataclasite and wall rock (20 µm to 3 cm in size) that appear to 'float' in an optically isotropic, reddish-brown to black, aphanitic matrix (Fig. 10e). The matrix lacks mica, epidote and amphibole and displays a submillimetre-scale banding, which is defined by compositional and clast-to-matrix variations. The pseudotachylites probably formed owing to high (seismic) strain rates which led to rapid frictional sliding (10⁻² to 1 m s⁻¹) and resulted in localized melting (>1000°C) (Spray 1995) of the wall rocks along the foliation-parallel fault networks. The friction melts are interpreted to have formed within host-rock below 300–350°C (i.e. at depths <11.5–10 km assuming a geothermal gradient of 30°C km⁻¹), as no argon loss was detected in the micas within the wall rocks (Sherlock *et al.* 2004).

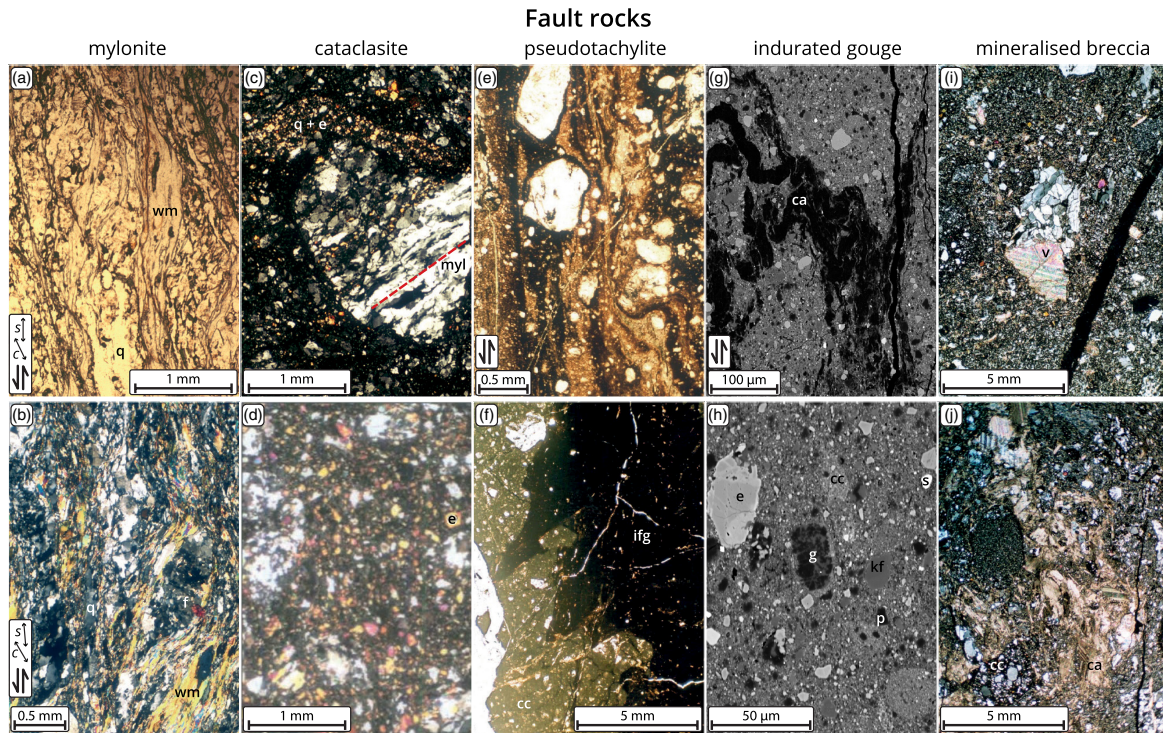


Fig. 10. Representative fault rock compositions and microstructures from the MFC. (a) High-strain mica-rich HSFZ mylonite with deformed interleaved quartzo-feldspathic, quartz (q) and white mica (wm) aggregates with sinistral S–C fabric (plane-polarized light (ppl) image). (b) VFZ quartzo-feldspathic mylonite with interleaved quartz ribbons (q), wrapped feldspar porphyroclasts (f) and white mica (wm) aggregated with sinistral S–C fabric (cross-polarized light (xpl) image). (c) HSFZ cataclasite with large clast of older mylonite (myl), both of which are cross-cut by quartz–epidote vein (q and e) (xpl image). (d) VFZ core cataclasite with clasts of finely comminuted gneiss, cataclasite, feldspar, quartz, epidote (e), chlorite and white mica set in a fine-grained epidote-rich matrix (xpl image). (e) HSFZ pseudotachylite with compositional flow banding and sinistral verging folds. The clasts are of quartz and feldspar from the protolith mylonite (ppl image). (f) Low-power view of irregular contact and injection structures of indurated fault gouge (ifg) into older highly altered cataclasite (cc) from the Verran Fault core (ppl image). (g) Backscatter SEM image of indurated fault gouge with sinistral folds Ca-smectite layers (ca), VF core. (h) Backscatter SEM image of indurated fault gouge from the Verran Fault core with fragments of epidote (e), pyrophyllite (p), cataclasite (cc), gneiss (g), K-feldspar (kf), titanite (t) and quartz within an ultrafine clay matrix (Ca-smectite and pyrophyllite). (i), (j) Images of typical calcite- and zeolite-mineralized breccias from the Verran Fault core with randomly oriented fragments of gneiss, cataclasite (cc), zeolite and calcite veins (v), feldspar, quartz and epidote within a matrix cemented by fine- to coarse-grained calcite (ca) and zeolite (both xpl images).

Indurated gouge

Well-cemented, black to dark brown, indurated gouge is only found within the VF core. In thin-section, the gouge appears to be a brown-coloured, clay-rich, isotropic paste containing subrounded clasts (0.1–0.5 mm in size) of cataclasite, quartz, epidote and, in places, feldspar. It displays a millimetre-scale colour banding owing to variations in grain size and the clast-to-matrix ratio. The gouge displays sharp, but highly irregular contacts with the adjacent cataclasite, which is cross-cut by millimetre-scale injection veins of gouge (Fig. 10f). SEM images (Fig. 10g and h) show the matrix to be composed of clasts of K-feldspar, epidote, quartz, chlorite, white mica and ‘newly’ formed pyrophyllite and ultracataclasite, which range from less than 1 to 10 μm in size. Anastomosing layers of Ca-smectite occur, typically 10–100 μm thick, and display micrometre-scale folds with consistent sinistral senses of vergence (Fig. 10g).

The dominance of cataclasite and presence of pyrophyllite indicate temperatures of *c.* 200°C. Ca-smectite, which probably formed from the breakdown of plagioclase, typically crystallizes at temperatures of between 80 and 150°C (Frey 1988). The indurated gouges are therefore considered to have formed at temperatures between *c.* 80 and 200°C, corresponding to depths of 3–7 km assuming an average geothermal gradient of 30°C km⁻¹.

Zeolite- and calcite-mineralized breccias

Zeolite- and calcite-cemented breccias and veins are widespread throughout the VFZ, the Verran Fault core and RF, but are limited in their development along the HSFZ. The breccias vary in colour

from pale grey, white and brown to brick-red or orange. They typically comprise randomly oriented, subangular to angular fragments (0.1–10 cm in size) of wall-rock set within a fine- to coarse-grained mineralized matrix of intergrown calcite and zeolite grains (Fig. 10i and j). The matrix comprises fibrous zeolite crystals (<0.1–1 mm in size) that form interlocking mosaics with calcite grains (0.1–2 cm in size). Gronlie *et al.* (1994) identified the zeolites as laumontite, stilbite and analcite based on XRD analyses. Randomly oriented calcite and zeolite veins (millimetres to centimetres thick) commonly cross-cut and also occur as clasts within the mineralized breccias, suggesting multiple vein generation during brecciation. The brittle deformation and preservation of Type 1 and 2 calcite deformation twins indicate temperatures of less than 200°C (Passchier and Trouw 2005). The coexistence of stilbite, laumontite and analcite indicates temperatures of between 100 and 160°C (Frey 1988). Therefore, the zeolite- and calcite-mineralized breccias are interpreted to have formed at depths of 3–5 km, assuming an average geothermal gradient of 30°C km⁻¹.

Grey and blue-grey gouges

All other fault rocks in the Verran Fault core are cross-cut by incohesive grey fault gouges, which range from 1 mm to 50 cm in thickness. They are very fine grained, containing clasts (0.5 mm to almost 1 cm in size) of cataclasite, zeolite and calcite breccias and granodiorite gneiss, together with pyrite mineralization. XRD analyses show the gouge matrix to be composed of Ca-smectite, chlorite, calcite and orthoclase.

The youngest blue–grey gouge is dominated by Ca-smectite (L.N. Warr, pers. comm. 2001), which suggests that the gouges formed at temperatures $<200^{\circ}\text{C}$ (Frey 1988) and depths <7 km assuming an average geothermal gradient of $30^{\circ}\text{C km}^{-1}$.

Discussion

Timing and regional significance of displacements along the MTFC

Devonian ductile sinistral shear (Fig. 11b, event 1) and possible earlier events

Widespread deformation along the HSFZ formed a 1 km-wide, ENE–WSW-trending, mylonitic, sinistral shear zone. The occurrence of pegmatite and microdiorite dykes, and extensive quartz veining, which are clearly overprinted by mylonite fabrics, and their increase in frequency towards the centre of the HSFZ, may indicate the presence of a precursor basement structure, such as a deep-seated igneous contact or a zone of dyking. The age of the overprinting sinistral mylonites is constrained by syntectonic mica overgrowths that have been dated at 406 ± 11 Ma using Ar–Ar geochronology (Fig. 11a; Sherlock *et al.* 2004). The earliest fault rocks along the VFZ are sparse mylonites formed during sinistral shear that are correlated with the Devonian-age HSFZ mylonites. The paucity of early ductile fault rocks along the VFZ may be due either to a lesser degree of exhumation along this fault strand and/or to the greater number and intensity of later fault movements here. Other long-lived natural fault zones such as the Great Glen–Walls Boundary Fault Zone in Scotland show a similar paucity of early ductile fault rocks (e.g. Stewart *et al.* 1999; Watts *et al.* 2007).

The ductile sinistral movements along the MTFC are broadly coeval with an unconformity in the Hitra Basin, which separates uppermost Silurian rocks from lower Devonian sedimentary rocks and also with top-to-the-SW movements along the Høybakken detachment (Fig. 1b). The latter structure is situated to the NW of the HSFZ and developed synchronously with the deposition of lower to middle Devonian sedimentary rocks (Séranne 1992; Robinson *et al.* 2004; Osmundsen *et al.* 2006). $^{40}\text{Ar}/^{39}\text{Ar}$ hornblende (386 ± 4 Ma) and mica (384 ± 3 and 381 ± 3 Ma) ages from the mylonites of the Høybakken detachment corroborate this suggestion (Kendrick *et al.* 2004). Top-to-the-SW ductile shear zones in the Banded Gneiss Complex (BGC) of SW Fosen are dated at 389 ± 6 and 386 ± 6 Ma (Rb–Sr, muscovite; Piasecki and Cliff 1988), and are also interpreted to be broadly contemporaneous with early movements along the MTFC and late Scandian orogenic collapse.

Séranne (1992) suggested that during the sinistral strike-slip movements, the Devonian basins formed in extensional detachments within releasing bends along the MTFC. Krabbendam and Dewey (1998) proposed a sinistral transtensional collapse model, with an increasing transtensional angle towards the MTFC, as an exhumation mechanism for the Western Gneiss Region. The structures and fabrics contemporaneous with the regional-scale antiformal structure that lies between the VFZ and the HSFZ in the basement gneisses are consistent with such transtension. The ductile, sinistral, strike-slip shear zones of the MTFC are then superimposed on this regional fold structure, but are still broadly compatible with the Krabbendam and Dewey (1998) model of transtensional collapse at *c.* 410–400 Ma. However, Terry *et al.* (2000) have suggested that regional shortening was still going on at depth at *c.* 400 Ma, coeval with extension and the deposition of sedimentary rocks in the Hitra Basin. Hence, the ductile sinistral movements on the MTFC were probably coeval with both the early stages of transtensional collapse at higher structural levels and the final stages of subduction of Baltica beneath Laurentia at depth.

Séranne (1992) proposed that on a large scale, the MTFC acted as a transfer between the Nordfjord–Sogn detachment in the SW and the Høybakken detachment. More recently, Braathen *et al.* (2000) suggested that north of the MTFC, bi-directional opposed extension led to the exhumation of the Central Norway Basement Window, whereas to the south unidirectional (top-to-the-WSW) extension dominated. As a result, the MTFC formed as a sinistral strike-slip transfer structure between the SW-dipping Høybakken detachment and the NE-dipping Kollstraumen detachment, to the SW and NE, respectively (see Braathen *et al.* 2000). Extensional movements along the Kollstraumen and Høybakken detachments related to late-orogenic collapse, dated at *c.* 390–381 Ma (Dallmeyer *et al.* 1992; Kendrick *et al.* 2004), are consistent with the timing of sinistral shear along the MTFC.

Permo-Carboniferous brittle sinistral transtension (Fig. 11b, event 2)

The regional-scale, ENE–WSW-trending, brittle sinistral faults that form the reactivated central part of the HSFZ and the broader VFZ are hard-linked by a series of north–south-trending extensional faults, the most prominent of which is the RF. All fault sets are associated with the development of quartz–epidote cataclases, local indurated fault gouge and pseudotachylite veins. The friction melts are much more prominent along the HSFZ and one has been dated by Sherlock *et al.* (2004) using Ar–Ar geochronology at 290 ± 10 Ma (Fig. 11a; early Permian, Artinskian). Moreover, a cataclase from the hanging wall of the Høybakken detachment zone provided Kendrick *et al.* (2004) with an Ar/Ar K-feldspar age of 321 ± 3 Ma (i.e. mid-Carboniferous). This mid-Carboniferous to early Permian sinistral event reactivated pre-existing gneissose and mylonitic foliations and established the regional-scale fault geometry of the MTFC (as seen in Fig. 1c). The calculated moment tensor (*P–T*) strain axes from the compiled fault slickenline data associated with this event are consistent with sinistral transtension (Fig. 11ci), with north–south compression and east–west extension.

Until the dating of the pseudotachylites by Sherlock *et al.* (2004), most researchers (e.g. Grønlie and Roberts 1989; Grønlie *et al.* 1991, 1994) viewed the sinistral, strike-slip brittle structures as being of probable latest Devonian or early Carboniferous age. The more precise Permo-Carboniferous age is almost exactly coeval with regional east–west extension and the development of the north–south-trending Oslo Rift (Pedersen *et al.* 1995; Heeremans *et al.* 1996; Torsvik *et al.* 1998; Ksienzyk *et al.* 2014). Torgersen *et al.* (2022) recently obtained a $^{40}\text{Ar}/^{39}\text{Ar}$ pseudotachylite plateau age of 294.6 ± 5.2 Ma from the reactivated Himdalen–Ørje Deformation Zone that lies close to the Oslo Graben. K-feldspar thermochronology in southern Norway has indicated rapid cooling with possibly 2–4 km of exhumation during Permo-Carboniferous time (Dunlap and Fossen 1998), and it seems likely that this is, at least in part, facilitated by the transtensional, brittle sinistral displacements along the MTFC in mid-Norway.

Mesozoic brittle faulting (Fig. 11b, events 3–6)

Following the Permo-Carboniferous events, the locus of reactivation shifted towards the VFZ during the Mesozoic, while the HSFZ remained largely inactive (Grønlie and Roberts 1989). A series of dip-slip and dextral strike-slip movements localized along the VFZ and were associated with multiphase brecciation, zeolite-calcite mineralization and gouge development. During dextral strike-slip along the ENE–WSW-trending VFZ, north–south-trending faults such as the Raudtindalen Fault were reactivated as sinistral strike-slip shears (Figs 6aiv and 11b, events 4 and 5; Grønlie and Roberts 1989; Grønlie *et al.* 1991). The calculated moment tensor (*P–T*) strain axes from the compiled fault slickenline data associated with

this event are consistent with dextral transtension (Fig. 11cii), with WNW–ESE compression and NNE–SSW extension.

The initial dip-slip normal movement along the VFZ (Fig. 11b, event 3) is interpreted to be of Jurassic age, based on the preservation of a 250 m-thick Jurassic succession in the hanging wall of the VF in the Beitstadfjorden Basin (Fig. 1b; Bøe and Bjerkli 1989). This event is also coeval with late Jurassic to early Cretaceous rifting in the Mid-Norwegian margin and North Sea (e.g. Fossen *et al.* 2017; Osmundsen and Péron-Pinvidic 2018; Osmundsen *et al.* 2021). Fossen *et al.* (2021) have suggested that widespread onshore faulting at this time precedes more focused rifting offshore. Offshore to the SW, the MTFC apparently defines the southern margin of the Møre Basin and comprises a series of fault-controlled ridges, highs and half-grabens (e.g. Grunnaleite and Gabrielsen 1995). The vertical throw of the near base Cretaceous is *c.* 5 km, which was interpreted to be related to late mid- to early Cretaceous rifting, as post-lower Cretaceous sedimentary rocks onlap onto the truncated fault blocks (Grunnaleite and Gabrielsen 1995). This interpretation is also consistent with the apatite fission-track (AFT) data obtained in transects across the MTFC by Redfield *et al.* (2005a).

Bøe and Bjerkli (1989) recognized a later phase of dextral strike-slip movement based upon north–south-trending folds and a series of sinistral offsets of the VF trace by north–south-trending faults within the Beitstadfjord Basin. These movements are consistent with the main phase of dextral strike-slip faulting and associated zeolite–calcite mineralization recognized during the present study (Fig. 11a and b, events 4 and 5). Bøe and Bjerkli (1989) also suggested that the north–south-trending folds were transected by the VF and inferred a later movement of possible early Cretaceous or Cenozoic age along the fault. This is consistent with the present study where later phases of post-zeolite, dextral strike-slip and dip-slip faulting are recognized in the Verran Fault core forming incohesive grey gouges (Fig. 11a). Similar relationships are recognized in the Edøyfjorden Basin to the SW of Fosen (Bøe and Bjerkli 1989) where both the VFZ and the HSFZ were recognized to have dip-slip normal displacements of no more than 1 km.

Several researchers have identified NE–SW compressional structures within the offshore Møre Basin of mid-Cenozoic age (e.g. Doré and Lundin 1996). A NW–SE compression across the MTFC is consistent with the most recent dip-slip (blue–grey gouge) movement phase recognized in this study (Fig. 11b, event 6). Other researchers have suggested an early Cretaceous inversion event along the MTFC (Bøe and Bjerkli 1989; Grunnaleite and Gabrielsen 1995). Fission-track dating of fluorite mineralization in one area, SE of Beitstadfjord, has yielded a late Cretaceous to Cenozoic mineralization age (Grønlie *et al.* 1990). Pascal and Gabrielsen (2001) noted that the MTFC separates an area with abundant Cenozoic compressional structures to the north (e.g. Møre Basin, Doré and Lundin 1996) from an area of relative tectonic quiescence to the south (e.g. northern North Sea). Stress modelling suggests that the MTFC acted as a shield to SE-directed ridge-push forces to the south (Pascal and Gabrielsen 2001), consistent with oblique or reverse movements. Pascal & Gabrielsen also postulated a recent dextral strike-slip component along the MTFC based on present-day stress patterns observed on the Norwegian continental shelf. Other researchers have provided evidence that the MTFC is still tectonically active offshore to the south of the Møre Basin (Ringdal 1983; Bungum *et al.* 1991; Lindholm *et al.* 1995; Hicks *et al.* 2000). The fault complex also separates crustal blocks with different present-day stress fields (e.g. Roberts and Myrvang 2004; Pascal *et al.* 2010).

There are both similarities and differences between the sequence of brittle deformation events suggested here (Fig. 11) and those along-strike to the SW for the MTFC in the region between Hitra

and Stad, as described by Hestnes *et al.* (2022) and Tartaglia *et al.* (2022). These researchers combined field observations, palaeostress inversion analyses and K–Ar dating of illite separated from selected fault zones to propose six brittle tectonic events. The clearest similarities are the recognition of the late Carboniferous–early Permian and Cretaceous events, whereas the Fosen Peninsula appears to lack any clear evidence for the proposed late Triassic–early Jurassic event with associated epidote–quartz mineralization. Furthermore, those parts of the MTFC and onshore mid-Norwegian margin studied by Hestnes *et al.* (2022) and Tartaglia *et al.* (2022) also lack evidence for the hydrothermal thorium-enriched carbonate veins and fault-related breccias of Permian age (e.g. Grønlie and Torsvik 1989; Grønlie *et al.* 1991). These differences may reflect regionally heterogeneous strain and fluid-flow histories along the MTFC and/or partitioning owing to the proximity of our study area to the main strike-slip fault strands initiated during the mid-Paleozoic. In addition, the study area is located inboard of an area of gently tapered continental crust (i.e. the offshore Trøndelag Platform) as opposed to the more sharply tapered Møre margin to the SW (e.g. Osmundsen and Redfield 2011). Further work is required to clarify these geological and temporal differences in faulting histories and associated mineralization episodes.

Reactivation and weakening

The present study clearly confirms that the MTFC preserves widespread evidence of repeated reactivation over long periods of geological time from the early Devonian to the Mesozoic and possibly as young as the Cenozoic, illustrating well that localization of deformation along major pre-existing structures can occur in preference to the formation of new fault zones during continental deformation (Fig. 11). The MTFC fault rocks show a progressive, decreasing-temperature evolution (Fig. 10), reflecting a progressive exhumation and shallowing of deformation processes through time. Later reactivations repeatedly localize into the highest strain regions of the earlier formed fault rocks in the fault core and, as displacements are relatively modest, fault rocks are preserved in sequence within the wall rocks adjacent to the fault core and have not, with the possible exception of the mylonites along the VFZ, been excised during later movements.

Studies of the HSFZ and the VFZ have shown that although both structures almost certainly initiated as sinistral ductile shear zones, they show significant differences in terms of their brittle fault attributes during the subsequent brittle sinistral reactivation. Thus, early formed fractures and faults in the centre of the VFZ tend to be longer and more connected over a wide zone (*c.* 500 m) compared with the shorter and less connected faults that developed in a much narrower zone (<100 m) along the HSFZ (Sleight 2001). This may explain why the VFZ experienced significantly higher volumes of fluid flow and associated calcite–zeolite mineralization during Mesozoic faulting episodes at depths <5 km. Major element geochemical analyses by Watts (2001) have shown that the cataclasites within the Verran Fault core are depleted (*c.* 15 wt%) in SiO₂ whereas cataclasites located immediately adjacent to the core are enriched (*c.* 5 wt%). This is interpreted to be the result of fluid-assisted diffusive mass transfer processes, in which silica was removed from the fault core and precipitated in voids within cataclasites of the damage zone. The exceptional fluid-rich conditions along the VF at this time may also explain the relative paucity of pseudotachylites along the VFZ compared with the relatively ‘dry’ nature of the HSFZ during the Permo-Carboniferous movements.

Such fluid-rich conditions would also be expected to have enhanced the onset of fluid-assisted reaction softening (of cataclasites) and fluid-assisted diffusional creep and weakening at depth (e.g. Stewart *et al.* 2000; Jefferies *et al.* 2006). This would

plausibly explain why later deformation localized along the VFZ whereas the HSFZ became inactive.

Conclusions

Detailed field and microstructural analyses have shown that the ENE–WSW-trending MTFC on Fosen comprises two major subvertical fault strands: the Hitra–Snåsa and Verran fault zones (HSFZ and VFZ). These two faults probably initiated as part of a single system of sinistral shear zones during the early Devonian following the emplacement of thrust sheets during the Scandian Orogeny. Permo–Carboniferous sinistral transtensional reactivation of the ENE–WSW-trending structures led to the development of cataclases and pseudotachylites together with the formation of north–south-trending faults, giving rise to the regional-scale brittle fault geometry of the MTFC. Several later phases of reactivation were focused preferentially along the VF and its north–south-linking structures during the Mesozoic and (possibly) Cenozoic, which were probably related to Mid- to Late Jurassic–Early Cretaceous rifting and subsequent Late Cretaceous–early Cenozoic opening of the North Atlantic. Displacements along the MTFC repeatedly localized along the earlier formed faults and foliations, illustrating that both the geometrical properties of the fault network and fault-zone weakening mechanisms are important controlling factors on fault reactivation. Extensive fracture-hosted fluid flow in the upper crust seems to have had a significant influence on the repeated localization of brittle deformation events, leading to the VFZ becoming the dominant structure in the MTFC and its offshore continuations during the Mesozoic and Cenozoic opening of the adjacent offshore basins of west–central Norway.

Scientific editing by Sarah Boulton

Acknowledgements We gratefully acknowledge the support of and many discussions with A. Doré and E. Lundin, and we very much appreciate the detailed and constructive review comments of E. Torgersen, an anonymous reviewer and Editor S. Boulton.

Author contributions LMW: investigation (lead), methodology (equal), validation (lead), writing – original draft (lead); REH: conceptualization (lead), funding acquisition (lead), project administration (lead), writing – original draft (supporting), writing – review & editing (lead); DR: conceptualization (equal), funding acquisition (supporting), investigation (supporting), writing – original draft (supporting), writing – review & editing (equal); JMS: investigation (supporting), methodology (supporting), writing – review & editing (supporting); RJW: formal analysis (lead), investigation (supporting), writing – review & editing (supporting)

Funding L.W. and J.S. gratefully acknowledge receipt of, respectively, NERC and Isle of Man studentships with additional support provided by Statoil (UK) Ltd (now Equinor UK).

Competing interests The authors declare that they have no known competing financial interests or personal relationships that could have appeared to influence the work reported in this paper.

Data availability All data generated or analysed during this study are included in this published article and its [supplementary information files](#).

References

- Allmendinger, R.W., Cardozo, N. and Fisher, D. 2012. *Structural Geology Algorithms: Vectors and Tensors in Structural Geology*. Cambridge University Press.
- Braathen, A., Nordgulen, Ø., Osmundsen, P.T., Andersen, T.B., Solli, A. and Roberts, D. 2000. Devonian, orogen-parallel, opposed extension of the Central Norwegian Caledonides. *Geology*, **28**, 615–618, [https://doi.org/10.1130/0091-7613\(2000\)28<615:DOOEIT>2.0.CO;2](https://doi.org/10.1130/0091-7613(2000)28<615:DOOEIT>2.0.CO;2)
- Braathen, A., Osmundsen, P.T., Nordgulen, Ø., Roberts, D. and Meyer, G. 2002. Orogen-parallel extension of the Caledonides in northern Central Norway: an overview. *Norwegian Journal of Geology*, **82**, 225–241.
- Bungum, H., Alsaker, A., Kvamme, L.B. and Hansen, R.A. 1991. Seismicity and seismotectonics of Norway and nearby continental shelf areas. *Journal of Geophysical Research*, **96**, 2249–2265, <https://doi.org/10.1029/90JB02010>
- Bøe, R. and Bjerkli, K. 1989. Mesozoic sedimentary rocks in Edøyfjorden and Beitstadfjorden, central Norway: implications for the structural history of the Møre–Trøndelag Fault Zone. *Marine Geology*, **87**, 287–299, [https://doi.org/10.1016/0025-3227\(89\)90066-2](https://doi.org/10.1016/0025-3227(89)90066-2)
- Bøe, R. and Sturt, B.A. 1991. Textural responses to evolving mass-flows: an example from the Devonian Asen Formation, central Norway. *Geological Magazine*, **128**, 99–109, <https://doi.org/10.1017/S0016756800018306>
- Bøe, R., Fossen, H. and Smelror, M. 2010. Mesozoic sediments and structures onshore Norway and in the coastal zone. *Norges geologiske undersøkelse Bulletin*, **450**, 15–32.
- Cobbold, P.R. and Quinquis, H. 1980. Development of sheath folds in shear regimes. *Journal of Structural Geology*, **2**, 119–126, [https://doi.org/10.1016/0191-8141\(80\)90041-3](https://doi.org/10.1016/0191-8141(80)90041-3)
- Dallmeyer, R.D., Johansson, L. and Möller, C. 1992. Chronology of high-pressure granulite-facies metamorphism, uplift, and deformation within the northern parts of the Western Gneiss Region, Norway. *Geological Society of America Bulletin*, **104**, 444–455, [https://doi.org/10.1130/0016-7606\(1992\)104<0444:COCHPG>2.3.CO;2](https://doi.org/10.1130/0016-7606(1992)104<0444:COCHPG>2.3.CO;2)
- Doré, A.G. and Lundin, E.R. 1996. Cenozoic compressional structures on the NE Atlantic margin: nature, origin and potential significance for hydrocarbon exploration. *Petroleum Geoscience*, **2**, 299–311, <https://doi.org/10.1144/petgeo.2.4.299>
- Doré, A.G., Lundin, E.R., Fichler, C. and Olesen, O. 1997. Patterns of basement structure and reactivation along the NE Atlantic margin. *Journal of the Geological Society, London*, **154**, 85–92, <https://doi.org/10.1144/gsjgs.154.1.0085>
- Dunlap, W.J. and Fossen, H. 1998. Early Paleozoic orogenic collapse, tectonic stability, and late Paleozoic continental rifting revealed through thermochronology of K-feldspars, southern Norway. *Tectonics*, **17**, 604–620, <https://doi.org/10.1029/98TC01603>
- Eide, E.A., Haabesland, N.E., Osmundsen, P.T., Andersen, T.B., Roberts, D. and Kendrick, M.A. 2005. Modern techniques and Old Red problems – determining the age of continental sedimentary deposits with ⁴⁰Ar/³⁹Ar provenance analysis in west–central Norway. *Norwegian Journal of Geology*, **85**, 133–149.
- Fossen, H., Khani, H.F., Faleide, J.I., Ksienzyk, A.H. and Dunlap, W.J. 2017. Post-Caledonian extension in the West Norway–northern North Sea region: the role of structural inheritance. *Geological Society, London, Special Publications*, **439**, 465–486, <https://doi.org/10.1144/SP439.6>
- Fossen, H., Ksienzyk, A.K., Rotevatn, A., Bauck, M.S. and Wemmer, K. 2021. From widespread faulting to localised rifting: evidence from K–Ar fault gouge dates from the Norwegian North Sea rift shoulder. *Basin Research*, **33**: 1934–1953, <https://doi.org/10.1111/bre.12541>
- Frey, M. 1988. *Low Temperature Metamorphism*. Blackie, Glasgow.
- Gabrielsen, R.H. and Ramberg, I.B. 1979. Fracture patterns in Norway from Landsat imagery: results and potential use. *Proceedings of the Norwegian Sea Symposium, Tromsø*, **23**, 1–28.
- Grønlie, A. and Roberts, D. 1989. Resurgent strike-slip duplex development along the Hitra–Snåsa and Verran Faults, Møre–Trøndelag Fault Zone, Central Norway. *Journal of Structural Geology*, **11**, 295–305, [https://doi.org/10.1016/0191-8141\(89\)90069-2](https://doi.org/10.1016/0191-8141(89)90069-2)
- Grønlie, A. and Torsvik, T.H. 1989. On the origin and age of hydrothermal, thorium-enriched carbonate veins and breccias in the Møre–Trøndelag Fault Zone, central Norway. *Norsk Geologisk Tidsskrift*, **69**, 1–19.
- Grønlie, A., Harder, V. and Roberts, D. 1990. Preliminary fission-track ages of fluorite mineralisation along fracture zones, inner Trondheimsfjord, Central Norway. *Norsk Geologisk Tidsskrift*, **70**, 173–178.
- Grønlie, A., Nilsen, B. and Roberts, D. 1991. Brittle deformation history of fault rocks on the Fosen Peninsula, Trøndelag, central Norway. *Norges geologiske undersøkelse Bulletin*, **421**, 39–57.
- Grønlie, A., Naeser, C.W., Naeser, N.D., Mitchell, J.G., Sturt, B.A. and Inneson, P.R. 1994. Fission track and K–Ar dating of tectonic activity in a transect across the Møre–Trøndelag Fault Zone, Central Norway. *Norsk Geologisk Tidsskrift*, **74**, 24–34.
- Grunnaleite, I. and Gabrielsen, R.H. 1995. The structure of the Møre Basin. *Tectonophysics*, **252**, 221–251, [https://doi.org/10.1016/0040-1951\(95\)00095-X](https://doi.org/10.1016/0040-1951(95)00095-X)
- Haabesland, N.E. 2002. *Sedimentarkitektur og migrasjon av sedimentære faciesenheter ved innfylling av et tektonisk aktivt halvgraben basseng, et eksempel fra Asenøy devonbassenget, Fosen, Trøndelag*. Cand. Scient. thesis, University of Oslo.
- Heeremans, M., Larsen, B.T. and Steel, H. 1996. Palaeostress reconstruction from kinematic indicators in the Oslo Graben, southern Norway: new constraints on the mode of rifting. *Tectonophysics*, **266**, 55–79, [https://doi.org/10.1016/S0040-1951\(96\)00183-7](https://doi.org/10.1016/S0040-1951(96)00183-7)
- Hestnes, Å., Gasser, D., Scheiber, T., Jacobs, J., van der Lelij, R., Schönenberger, J. and Ksienzyk, A.K. 2022. The brittle evolution of western Norway – a space–time model based on fault mineralisations, K–Ar fault gouge dating and palaeostress analysis. *Journal of Structural Geology*, **160**, <https://doi.org/10.1016/j.jsg.2022.104621>
- Hicks, E., Bungum, H. and Lindholm, C. 2000. Stress inversions of earthquake focal mechanism solutions from onshore and offshore Norway. *Norwegian Journal of Geology*, **80**, 235–250.

- Holdsworth, R.E., Butler, C.E. and Roberts, A.M. 1997. The recognition of reactivation during continental deformation. *Journal of the Geological Society, London*, **154**, 73–78, <https://doi.org/10.1144/gsjgs.154.1.0073>
- Hollocher, K., Robinson, P., Walsh, E. and Roberts, D. 2012. Geochemistry of amphibolite-facies volcanics and gabbros of the Støren Nappe in extensions west and southwest of Trondheim, Western Gneiss Region, Norway: a key to correlations and paleotectonic settings. *American Journal of Science*, **312**, 357–416, <https://doi.org/10.2475/04.2012.01>
- Imber, J., Holdsworth, R.E., Butler, C.A. and Strachan, R.A. 2001. A reappraisal of the Sibson–Scholz fault zone model: the nature of the frictional–viscous ('brittle–ductile') transition along a long-lived crustal-scale fault, Outer Hebrides, Scotland. *Tectonics*, **20**, 601–624, <https://doi.org/10.1029/2000TC001250>
- Jefferies, S.P., Holdsworth, R.E., Shimamoto, T., Takagi, H., Lloyd, G.E. and Spiers, C.J. 2006. Origin and mechanical significance of foliated cataclastic rocks in the cores of crustal-scale faults: Examples from the Median Tectonic Line, Japan. *Journal of Geophysical Research: Solid Earth*, **111**, B12303, <https://doi.org/10.1029/2005JB004205>
- Johansson, L. 1986. *Basement and cover relationships in the Vestranden–Grong–Olden region, Central Scandinavian Caledonides: age relationships, structures and regional correlation*. PhD thesis, University of Lund.
- Kendrick, M.A., Eide, E.A., Roberts, D. and Osmundsen, P.T. 2004. The Mid–Late Devonian Høybakken Detachment, Central Norway: ⁴⁰Ar/³⁹Ar evidence for prolonged late/post-Scandian extension and uplift. *Geological Magazine*, **141**, 329–344, <https://doi.org/10.1017/S0016756803008811>
- Krabbendam, M. and Dewey, J.F. 1998. Exhumation of UHP rocks by transtension in the Western Gneiss Region, Scandinavian Caledonides. *Geological Society, London, Special Publications*, **135**, 159–181, <https://doi.org/10.1144/GSL.SP.1988.135.01.11>
- Ksienzyk, A.K., Dunkl, I., Jacobs, J., Fossen, H. and Kohlmann, F. 2014. From orogen to passive margin: constraints from fission track and (U–Th)/He analyses on Mesozoic uplift and fault reactivation in SW Norway. *Geological Society, London, Special Publications*, **390**, 679–702, <https://doi.org/10.1144/SP390.27>
- Lidmar-Bergström, K., Ollier, C.D. and Sulebak, J.R. 2000. Landforms and uplift history of southern Norway. *Global and Planetary Change*, **24**, 211–231, [https://doi.org/10.1016/S0921-8181\(00\)00009-6](https://doi.org/10.1016/S0921-8181(00)00009-6)
- Lindholm, C.D., Bungum, H., Bratli, R.K., Aadnøy, B.S., Dahl, N., Tørudbakken, B. and Atakan, K. 1995. Crustal stress in the northern North Sea as inferred from borehole breakouts and earthquake focal mechanisms. *Terra Nova*, **7**, 51–59, <https://doi.org/10.1111/j.1365-3121.1995.tb00667.x>
- Manatschal, G., Lavier, L. and Chenin, P. 2014. The role of inheritance in structuring hyperextended rift systems: some considerations based on observations and numerical modeling. *Gondwana Research*, **27**, 140–164, <https://doi.org/10.1016/j.gr.2014.08.006>
- Marrett, R.A. and Allmendinger, R.W. 1990. Kinematic analysis of fault-slip data. *Journal of Structural Geology*, **12**, 973–986, [https://doi.org/10.1016/0191-8141\(90\)90093-E](https://doi.org/10.1016/0191-8141(90)90093-E)
- Möller, C. 1988. Geology and metamorphic evolution of the Roan area, Vestranden, Western Gneiss Region, Central Norwegian Caledonides. *Norges geologiske undersøkelse Bulletin*, **413**, 1–31.
- Nasuti, A., Pascal, C., Ebbing, J. and Tønnesen, J.F. 2011. Geophysical characterisation of two segments of the Møre–Trøndelag Fault Complex, Mid Norway. *Solid Earth*, **2**, 125–134, <https://doi.org/10.5194/se-2-125-2011>
- Nordgulen, Ø., Braathen, A., Corfu, F. and Osmundsen, P.T. 2002. Polyphase kinematics and geochronology of the Kollstraumen detachment. *Norwegian Journal of Geology*, **82**, 299–316.
- Norton, M.G., McClay, K.R. and Way, N.A. 1987. Tectonic evolution of Devonian basins in northern Scotland and southern Norway. *Norsk Geologisk Tidsskrift*, **67**, 323–338.
- Olsen, E., Gabrielsen, R.H., Braathen, A. and Redfield, T.F. 2007. Fault systems marginal to the Møre–Trøndelag Fault Complex, Osen–Vikna area, Central Norway. *Norwegian Journal of Geology*, **87**, 59–73.
- Osmundsen, P.T. and Péron-Pinvidic, G. 2018. Crustal-scale fault interaction at rifted margins and the formation of domain-bounding breakaway complexes: insights from offshore Norway. *Tectonics*, **37**, 935–964, <https://doi.org/10.1002/2017TC004792>
- Osmundsen, P.T. and Redfield, T.F. 2011. Crustal taper and topography at passive continental margins. *Terra Nova*, **23**, 349–361, <https://doi.org/10.1111/j.1365-3121.2011.01014.x>
- Osmundsen, P.T., Braathen, A., Nordgulen, Ø., Roberts, D., Meyer, G.B. and Eide, E. 2003. The Devonian Nesna shear zone and adjacent gneiss-cored culminations, North–Central Norwegian Caledonides. *Journal of the Geological Society, London*, **160**, 137–150, <https://doi.org/10.1144/0016-764901-173>
- Osmundsen, P.T., Eide, E.A. et al. 2006. Kinematics of the Høybakken detachment zone and the Møre–Trøndelag Fault Complex, central Norway. *Journal of the Geological Society, London*, **163**, 303–318, <https://doi.org/10.1144/0016-764904-129>
- Osmundsen, P.T., Péron-Pinvidic, G. and Bunkholt, H. 2021. Rifting of collapsed orogens: Successive incision of continental crust in the proximal margin offshore Norway. *Tectonics*, **40**, e2020TC006283, <https://doi.org/10.1029/2020TC006283>
- Pascal, C. and Gabrielsen, R.H. 2001. Numerical modelling of Cenozoic stress patterns in the Mid Norwegian Margin and the northern North Sea. *Tectonics*, **20**, 585–599, <https://doi.org/10.1029/2001TC900007>
- Pascal, C., Roberts, D. and Gabrielsen, R.H. 2010. Tectonic significance of present-day stress relief phenomena in formerly glaciated regions. *Journal of the Geological Society, London*, **167**, 363–371, <https://doi.org/10.1144/0016-76492009-136>
- Passchier, C.W. and Trouw, R.A.J. 2005. *Microtectonics*, 2nd edn. Springer, Berlin.
- Pedersen, L.E., Heaman, L.M. and Holm, P.M. 1995. Further constraints of the temporal evolution of the Oslo Rift from precise U–Pb zircon dating in the Siljan–Skrim area. *Lithos*, **34**, 301–315, [https://doi.org/10.1016/0024-4937\(94\)00014-S](https://doi.org/10.1016/0024-4937(94)00014-S)
- Peron-Pinvidic, G. and Osmundsen, P.T. 2020. From orogeny to rifting: insights from the Norwegian 'reactivation phase'. *Nature Research, Scientific Reports*, **10**, 1–7, <https://doi.org/10.1038/s41598-020-71893-z>
- Petit, J.P. 1987. Criteria for the sense of movement on fault surfaces in brittle rocks. *Journal of Structural Geology*, **9**, 597–608, [https://doi.org/10.1016/0191-8141\(87\)90145-3](https://doi.org/10.1016/0191-8141(87)90145-3)
- Phillips, T.B., Jackson, C.A.L., Bell, R.E., Duffy, O.B. and Fossen, H. 2016. Reactivation of intrabasement structures during rifting: a case study from offshore southern Norway. *Journal of Structural Geology*, **91**, 54–73, <https://doi.org/10.1016/j.jsg.2016.08.008>
- Piasecki, M.A.J. and Cliff, R.A. 1988. Rb–Sr dating of strain-induced mineral growth in two ductile shear zones in the Western Gneiss Region of Nord-Trøndelag, Central Norway. *Norges geologiske undersøkelse Bulletin*, **413**, 33–50.
- Redfield, T.F. and Osmundsen, P.T. 2009. The Tjellefonna fault system of western Norway: linking late-Caledonian extension, post-Caledonian normal faulting, and Tertiary rock-column uplift with the landslide-generated tsunami event of 1756. *Tectonophysics*, **474**, 106–123, <https://doi.org/10.1016/j.tecto.2009.02.006>
- Redfield, T.F. and Osmundsen, P.T. 2013. The long-term topographic response of a continent adjacent to a hyperextended margin: a case study from Scandinavia. *Geological Society of America Bulletin*, **125**, 184–200, <https://doi.org/10.1130/B30691.1>
- Redfield, T.F., Torsvik, T.H., Andriessen, P.A.M. and Gabrielsen, R.H. 2004. Mesozoic and Cenozoic tectonics of the Møre–Trøndelag Fault Complex, central Norway: constraints from new apatite fission track data. *Physics and Chemistry of the Earth*, **29**, 673–682, <https://doi.org/10.1016/j.pce.2004.03.005>
- Redfield, T.F., Braathen, A., Gabrielsen, R.H., Osmundsen, P.T., Torsvik, T. and Andriessen, P.A.M. 2005a. Late Mesozoic to Early Cenozoic components of vertical separation across the Møre–Trøndelag Fault Complex, Norway. *Tectonophysics*, **395**, 233–249, <https://doi.org/10.1016/j.tecto.2004.09.012>
- Redfield, T.F., Osmundsen, P.T. and Hendriks, B.W.H. 2005b. The role of fault reactivation and growth in the uplift of western Fennoscandia. *Journal of the Geological Society, London*, **162**, 1013–1030, <https://doi.org/10.1144/0016-764904-149>
- Ringdal, F. 1983. Seismicity of the North Sea area. In: Ritsema, A.R. and Garpinar, A. (eds) *Seismicity and Seismic Risk in the Offshore North Sea Area*. NATO Advanced Research Workshop. D. Reidel, 53–75.
- Roberts, D. 1983. Devonian tectonic deformation in the Norwegian Caledonides and its regional perspectives. *Norges geologiske undersøkelse Bulletin*, **380**, 85–96.
- Roberts, D. 1986. Structural–photogeological and general features of the Fosen–Namsos Western Gneiss Region of Central Norway. *Norges geologiske undersøkelse Bulletin*, **407**, 13–25.
- Roberts, D. 1998. High-strain zones from meso- to macro-scale at different structural levels, Central Norwegian Caledonides. *Journal of Structural Geology*, **20**, 111–119, [https://doi.org/10.1016/S0191-8141\(97\)00082-5](https://doi.org/10.1016/S0191-8141(97)00082-5)
- Roberts, D. and Gee, D.G. 1985. An introduction to the structure of the Scandinavian Caledonides. In: Gee, D.G. and Sturt, B.A. (eds) *The Caledonide Orogen – Scandinavia and Related Areas*. Wiley, Chichester, 55–68.
- Roberts, D. and Myrvang, A. 2004. Contemporary stress orientation features in bedrock, Trøndelag, central Norway, and some regional implications. *Norges geologiske undersøkelse Bulletin*, **442**, 53–63.
- Roberts, D. and Stephens, M.B. 2000. Caledonian orogenic belt. *Geological Survey of Finland, Special Paper*, **28**, 79–104 and 146–159.
- Robinson, P., Tucker, R.D., Solli, A., Terry, M.P., Krogh, T.E., Gee, D.G. and Nordgulen, Ø. 2004. Scandian thrusting and extension in the Western Gneiss Region, Sor-Trøndelag and Møre og Romsdal, Norway. *GFF Abstract Volume*, **126**, 84–85 [abstract].
- Séranne, M. 1992. Late Palaeozoic kinematics of the Møre–Trøndelag Fault Zone and adjacent areas, Central Norway. *Norsk Geologisk Tidsskrift*, **72**, 141–158.
- Sherlock, S.C., Watts, L.M., Holdsworth, R.E. and Roberts, D. 2004. Dating fault reactivation by Ar/Ar laserprobe: an alternative view of apparently cogenetic mylonite–pseudotachylite assemblages. *Journal of the Geological Society, London*, **161**, 335–338, <https://doi.org/10.1144/0016-764903-160>
- Siedlecka, A. 1975. Old Red Sandstone lithostratigraphy and sedimentation of the outer Fosen area, Trondheim region. *Norges geologiske undersøkelse*, **321**, 1–35.
- Sleight, J.M. 2001. *Fracture characteristics from two reactivated basement fault zones: examples from Norway and Shetland*. PhD thesis, University of Durham.
- Solli, A., Bugge, T. and Thorsnes, T. 1997. *Geologisk kart over Norge, berggrunnskart Namsos, M 1:250 000*. Norges geologiske undersøkelse.
- Sommaruga, A. and Bøe, R. 2002. Geometry and subcrop maps of shallow Jurassic basins along the Mid-Norway coast. *Marine and Petroleum Geology*, **19**, 1029–1042, [https://doi.org/10.1016/S0264-8172\(02\)00113-7](https://doi.org/10.1016/S0264-8172(02)00113-7)

- Spray, J.G. 1995. Pseudotachylite controversy: fact or friction? *Geology*, **23**, 1119–1122, [https://doi.org/10.1130/0091-7613\(1995\)023<1119:PCFOF>2.3.CO;2](https://doi.org/10.1130/0091-7613(1995)023<1119:PCFOF>2.3.CO;2)
- Steel, R., Siedlecka, A. and Roberts, D. 1985. The Old Red Sandstone basins of Norway and their deformation: a review. In: Gee, D.G. and Sturt, B.A. (eds) *The Caledonide Orogen – Scandinavia and Related Areas*. Wiley, Chichester, 293–315.
- Steltenpohl, M.G., Moecher, D., Andresen, A., Ball, J., Mager, S. and Hames, W.E. 2011. The Eidsfjord shear zone, Lofoten–Vesterålen, north Norway: an Early Devonian, paleoseismogenic low angle normal fault. *Journal of Structural Geology*, **33**, 1023–1043, <https://doi.org/10.1016/j.jsg.2011.01.017>
- Stewart, M., Strachan, R.A. and Holdsworth, R.E. 1999. Structure and early kinematic history of the Great Glen Fault Zone, Scotland. *Tectonics*, **18**, 326–342, <https://doi.org/10.1029/1998TC900033>
- Stewart, M., Holdsworth, R.E. and Strachan, R.A. 2000. Deformation processes and weakening mechanisms within the frictional–viscous transition zone of major crustal faults: insights from the Great Glen Fault Zone, Scotland. *Journal of Structural Geology*, **22**, 543–560, [https://doi.org/10.1016/S0191-8141\(99\)00164-9](https://doi.org/10.1016/S0191-8141(99)00164-9)
- Sæther, O.M., Roberts, D. and Reimann, C. 2005. Structural control of strontium concentrations in stream sediments: an example from major fault zones in central Norway. *Geochemistry, Exploration, Environment, Analysis*, **5**, 183–188, <https://doi.org/10.1144/1467-7873/03-056>
- Tartaglia, G., Cerrato, A., Scheiber, T., van der Lelij, R., Schönerberger, J. and Viola, G. 2022. Time-constrained multiphase brittle tectonic evolution of the onshore mid-Norwegian passive margin. *Geological Society of America Bulletin*, <https://doi.org/10.1130/B36312.1>
- Terry, M.P., Robinson, P., Hamilton, M.A. and Jercinovic, M.J. 2000. Monazite geochronology of UHP and HP metamorphism, deformation, and exhumation, Nordøyane, Western Gneiss Region, Norway. *American Mineralogist*, **85**, 1651–1664, <https://doi.org/10.2138/am-2000-11-1208>
- Torgersen, E., Gabrielsen, R., Ganerød, M., Van der Lelij, R., Schönerberger, J., Nystuen, J. and Brask, S. 2022. Repeated brittle reactivations of a pre-existing plastic shear zone: Combined K–Ar and ^{40}Ar – ^{39}Ar geochronology of the long-lived (>700 Ma) Himdalen–Ørje Deformation Zone, SE Norway. *Geological Magazine*, <https://doi.org/10.1017/S0016756822000966>
- Torsvik, T.H., Eide, E.A., Meert, J.G., Smethurst, M.A. and Walderhaug, H. 1998. The Oslo Rift: new palaeomagnetic and ^{40}Ar – ^{39}Ar age constraints. *Geophysical Journal International*, **135**, 1045–1059, <https://doi.org/10.1046/j.1365-246X.1998.00687.x>
- Tucker, R.D., Robinson, P. *et al.* 2004. Thrusting and extension in the Scandian hinterland, Norway: new U–Pb ages and tectonostratigraphic evidence. *American Journal of Science*, **304**, 477–532, <https://doi.org/10.2475/ajs.304.6.477>
- Watts, L.M. 2001. *The Walls Boundary Fault Zone and the Møre-Trøndelag Fault Complex: a case study of two reactivated fault zones*. PhD thesis, University of Durham.
- Watts, L.M., Holdsworth, R.E., Sleight, J.A., Strachan, R.A. and Smith, S.A.F. 2007. The movement history and fault rock evolution of a reactivated crustal-scale strike-slip fault: the Walls Boundary Fault Zone, Shetland. *Journal of the Geological Society, London*, **164**, 1037–1058, <https://doi.org/10.1144/0016-76492006-156>
- Wilson, R.W., McCaffrey, K.J.W., Holdsworth, R.E., Imber, J., Jones, R.R., Welbon, A.I.F. and Roberts, D. 2006. Complex fault patterns, transtension and structural segmentation of the Lofoten Ridge, Norwegian margin: using digital mapping to link onshore and offshore geology. *Tectonics*, **25**, TC4018, <https://doi.org/10.1029/2005TC001895>
- Wilson, R.W., Holdsworth, R.E., Wild, L.E., McCaffrey, K.J.W., England, R.W., Imber, J. and Strachan, R.A. 2010. Basement-influenced rifting and basin development: a reappraisal of post-Caledonian faulting patterns in the North Coast Transfer Zone, Scotland. *Geological Society, London, Special Publications*, **335**, 795–826, <https://doi.org/10.1144/SP335.32>
- Yardley, B.W.D. 1989. *An Introduction to Metamorphic Petrology*. Longman Scientific and Technical, London.